Long-term exhumation of landscapes along the Pacific-North American plate boundary as inferred from apatite (U-Th)/He and ArcGIS analyses

Jamie Todd Buscher

Dissertation submitted to the faculty of the Virginia Polytechnic Institute and State University in partial fulfillment of the requirements for the degree of

Doctor of Philosophy in Geosciences

Committee
James A. Spotila, Chair
John A. Hole
Richard D. Law
Kenneth A. Eriksson

May 3, 2007
Blacksburg, Virginia

Keywords: exhumation, (U-Th)/He dating, ArcGIS, southern San Andreas fault, Aleutian subduction zone

Long-term exhumation of landscapes along the Pacific-North American plate boundary as inferred from apatite (U-Th)/He and ArcGIS analyses

Jamie Todd Buscher

Abstract

The Pacific-North American plate boundary is typified by transpression and convergence, yet the relationship between interplate deformation and long-term crustal shortening is not fully understood. The continuous belt of rugged topography that extends along the entire plate boundary is generally associated with oblique tectonic plate motion, strong interplate coupling, and terrane accretion, but relating plate boundary orogenesis to variations in plate geometry and behavior requires detailed case studies. The northern San Gabriel Mountains along the San Andreas fault and the Chugach-Kenai Mountains above the Aleutian subduction zone are located along highly tectonically active sections of the Pacific-North American plate boundary and have not been studied from the context of long-term landscape development. To determine whether mountain building along these sections of the plate boundary reflects recent, rapid exhumation as observed in bordering mountain belts, low-temperature thermochronometry and topographic analyses were applied to each area. In the northern San Gabriel Mountains, apatite (U-Th)/He ages are >10 Ma along narrow crystalline ridges topped by low-slope erosional surfaces located within

~5 km of the San Andreas fault zone. In the Chugach-Kenai Mountains, the youngest apatite (U-Th)/He ages (~5 Ma) are an order of magnitude older than those from the Yakutat collision zone to the east, despite the presence of a continuous swath of glaciated, rugged topography between the two areas. Exhumation rates inferred from these ages are <1 mm/yr, suggesting that there has been minimal recent denudation in the northern San Gabriel and Chugach-Kenai Mountains. The lack of evidence for recent mountain building in both of these case studies implies that interplate deformation is heterogeneous and that other factors (secondary structures, climate) besides plate kinematics and topographic character must be considered for understanding landscape development.

Acknowledgements

My inspiration to study geology and ultimately pursue a Ph.D. has taken me to three institutions of higher learning and some of the most beautiful locations in the world, but this experience would not have been possible without the support and guidance of some very important people in my life both within and outside of the academic community. My passion for traveling to distant lands to study rocks came from my family. My dad was always enthusiastic and supportive of my higher education endeavors and constantly reminded me of how exciting it is to observe and study nature. My mom was always there to support my field adventures in every way, making me feel at home with a laugh and a smile. My sister kept me aware of the creative side of my brain and had similar academic goals that were motivation for my higher education pursuits. The FergieSmiths and Ryans always expressed an interest in my studies and travels with a hint of sarcasm, while my grandma would always take my side. Grandma, you are dearly missed and I wish you were here.

The path to my Ph.D. started in the Geology Department at Pasadena City College. In my first semester as a full-time student, I needed one course to complete my schedule and by chance ended up taking an introductory geology class with Mr. Gerald Lewis, the teacher who sparked my interest in rocks and ultimately motivated me to study geology. His vast knowledge of geology in the western United States and stimulating stories from the field, all taught with a taste

of sarcasm, inspired me to take more courses in the department and pursue a career in geology. Dr. David Douglass provided insight on transferring to four-year universities and life as a graduate student, led field trips throughout the western United States with Mr. Gerald Lewis, and strongly supported my decision to attend graduate school. Dr. Janet Gordon taught the most challenging and comprehensive introductory geology class that I have seen at any school, inspiring me to take field geology classes in the department.

After Pasadena City College, I was a student in the Earth and Space Sciences Department at UCLA where I became interested in crustal deformation and mountain building. Dr. An Yin taught my favorite undergraduate class, structural geology, and has been one of the most important and influential mentors to me by helping with decisions about graduate schools, advisors, and my career and always offering assistance for anything at any time. Dr. Eric Cowgill exposed me to the challenges of graduate field research by inviting me to work as a field assistant in China and offered important advice on choosing a graduate school and advisor.

After working for three years in the geotechnical industry, I attended graduate school for my M.S. and ultimately my Ph.D. in the Geosciences Department at Virginia Tech, where my most significant personal achievements as a student, scientist, and professional took place. Dr. James Spotila was my advisor for both my M.S. and Ph.D. and was primarily responsible for my

development from a novice scientist with a three year absence from academia to a professional researcher. His drive to create interesting and challenging research projects and to maintain extremely high academic standards pushed me to achieve skills as a writer, drafter, and scientist that I had not previously accomplished. My committee members, Dr. John Hole, Dr. Richard Law, and Dr. Kenneth Eriksson, all sparked stimulating discussions both in and out of the classroom and offered excellent advice for my research and life beyond graduate school.

Support for my learning experience at Virginia Tech extended beyond my committee members. Aaron Berger was always there for scientific discussions and input on projects and constantly reminded me how exciting it is to be a geologist. Ryan McAleer was exceptional at uncovering software secrets and finding a way to make me laugh even when it was late night crunch time in Derring Hall. Dylan Ward showed me that it was possible to do twice as much work as I normally do in half the time. Connie Lowe, my mother away from home, was always patient while explaining procedures that I should have already known from the previous year. She was always on the side of the students, fighting different components of the department or university, and was always available to talk to for school business or as a friend. The administrative and technical staff were always there to provide prompt help with a smile and were extremely nice even when I had difficulty remembering how to fill out forms or follow procedures that I had done for years. The faculty were always available for

discussions about science and life beyond graduate school, leaving the door open for friendships and collaborations. I have truly enjoyed my time at Virginia Tech and if I had to do everything over again, I would be right back here in Blacksburg.

Attributions

Chapter two was submitted to *Tectonics* as “Buscher, J.T. and J.A. Spotila, Near-field response to transpression along the southern San Andreas fault, based on exhumation of the northern San Gabriel Mountains, southern California.” J.T. Buscher collected and prepared samples to be dated by the (U-Th)/He technique, conducted ArcGIS analyses, developed ideas for the study, wrote the manuscript, and created the figures and tables. J.A. Spotila developed the original idea for the study, secured funding for the project, analyzed samples with the (U-Th)/He technique, and provided feedback on earlier versions of the manuscript.

Chapter three was submitted to *AGU, Chapman Monograph* as “Buscher, J.T., A.L. Berger, and J.A. Spotila, Exhumation in the Chugach-Kenai Mountain belt above the Aleutian subduction zone, southern Alaska.” J.T. Buscher collected and prepared samples to be dated by the (U-Th)/He technique, conducted ArcGIS analyses, developed ideas for the study, wrote the manuscript, and created the figures and tables. A.L. Berger helped collect and prepare samples to be dated by the (U-Th)/He technique and provided thoughtful comments on earlier versions of the manuscript. J.A. Spotila developed the original idea for the study, secured funding for the project, analyzed samples with the (U-Th)/He technique, and provided feedback on earlier versions of the manuscript.

Table of Contents

Chapter 3

List of Figures

Chapter 2

Chapter 3

List of Tables

Chapter 2

Chapter 3

Chapter 1

Introduction

The active Pacific-North American plate boundary in southern California and southern Alaska is dominated by active faulting and mountainous topography, but it is not fully understood how the contribution of plate convergence is transformed into vertical deformation. High obliquity (>20°) along the San Andreas fault section of the plate boundary has produced the rugged Transverse Ranges in southern California, and active subduction and collision at the plate interface in southern Alaska has created the highest coastal mountain range in the world. Although this plate boundary is characterized by extensive mountain building, evidence from (U-Th)/He and ArcGIS analyses suggest that deformation is not uniform along strike despite little variation in plate geometry and topography.

Data from the northern San Gabriel and Chugach-Kenai Mountains in southern California and Alaska, respectively, suggest there has been minimal exhumation in these ranges despite evidence for active deformation in adjacent blocks. Young low-temperature thermochronometry ages (<2 Ma) from the San Bernardino and San Gabriel Mountains suggest that recent, rapid exhumation has been generated from the San Andreas fault [*Spotila et al.*, 2001; *Blythe et al.*, 2002], yet (U-Th)/He ages located immediately adjacent to the fault zone in the

northern San Gabriel Mountains to the west are >4 Ma. Young (U-Th)/He ages from the Chugach (<0.5 Ma) and Fairweather Mountains (1-2 Ma) suggest there has been rapid exhumation of coastal southern Alaska [*Berger and Spotila*, 2006; *McAleer and Spotila*, in prep.], but ages from the Chugach-Kenai Mountains in the hanging wall of the Aleutian subduction zone to the west are >4 Ma. The presence of old ages suggests that long-term deformation has been diffuse in both of these portions of the Pacific-North America plate boundary despite topographic evidence suggesting otherwise.

Rugged landscapes are maintained between the northern San Gabriel and Chugach-Kenai Mountains and adjacent rapidly exhuming mountain blocks, but ArcGIS analyses show that topographic variations exist. Peak elevations from both the northern San Gabriel and Chugach-Kenai Mountains are ~2000 m lower than adjacent peaks where active deformation is inferred [*Spotila et al.*, 2001; *Blythe et al.*, 2002; *Spotila et al.*, 2004; *Bruhn et al.*, 2004; *Berger et al.*, in prep.; *Meigs et al.*, in prep.]. These significantly lower peak elevations suggest there has been less surface uplift and/or more erosional downwearing than neighboring regions. High slopes are found adjacent to tall peaks in the central portion of both the northern San Gabriel and Chugach-Kenai Mountains, but there is no correlation between slope and the location of active structures. High slopes loosely correlate with maximum precipitation in the northern San Gabriel

Mountains but vigorous glaciation of the entire Chugach-Kenai Mountains suggests that slope is controlled by other factors.

The anomalously high (U-Th)/He ages and relatively low peak elevations of these two regions suggest that deformation along active plate boundaries is heterogeneous. Evidence for minimal exhumation along these sections of the Pacific-North American plate boundary expected to be actively deforming imply that vertical deformation is diffuse or redistributed to adjacent areas where rapid exhumation is observed. Although rugged topography generally reflects active shortening, it is critical to quantify the timing and kinematics of deformation to fully understand landscape development along entire plate boundaries. This dissertation addresses these case studies individually to shed light on the varying distribution of vertical deformation along the Pacific-North American plate boundary.

Chapter 2

Near-field response to transpression along the southern San Andreas fault, based on exhumation of the northern San Gabriel Mountains, southern California

JAMIE T. BUSCHER and JAMES A. SPOTILA

Department of Geosciences, Virginia Polytechnic Institute and State University, Blacksburg, Virginia 24061, USA

Submitted to *Tectonics*, 2007

Abstract

Near-field mountain building is common along transpressive faults, but how vertical deformation relates to oblique plate motion versus local structural complexity has not been universally established. We have investigated the mechanisms of exhumation along the southern San Andreas fault in the northern San Gabriel Mountains to examine the effects of pure-shear dominated transpression (obliquity >20^{o}). Although rugged topography suggests near-field uplift, low-temperature thermochronometry indicates minimal exhumation. Apatite (U-Th)/He ages are >10 Ma along narrow ridges within the fault zone, implying near-field rock uplift is not pervasive along this oblique plate boundary. Ages farther from the fault are younger (~5 Ma) and suggest a deformation event occurred during the transition of activity from the San Gabriel fault to the modern San Andreas strand. These results reveal a heterogeneous crustal response to transpression and imply that secondary structures or geometrical complexities play a primary role in near-field bedrock uplift along transpressive faults.

Introduction

The distribution of deformation along plate boundaries is revealing for understanding the dynamics and rheology of the lithosphere [*England and Houseman*, 1985; *Molnar*, 1988]. Along transpressive plate boundaries, oblique convergence is accommodated by shortening that generally leads to rock uplift

directly along strike-slip fault zones. Numerous observations support this generality. Flower or palm-shaped structures and local pop-ups mapped along strike-slip fault zones suggest pure-shear deformation is concentrated within fault zones [*Sylvester*, 1988; *Bürgmann*, 1991; *Vauchez and Nicolas*, 1991]. Near-field bedrock uplift (i.e. within ~10-20 km of a fault) at an even larger scale is illustrated by rapid cooling of crustal slivers along transpressional fault zones [*Foster et al*., 1994; *Spotila et al*., 2001; *Thomson*, 2002]. Wholesale rock uplift at transpressive boundaries is further indicated by orogenesis that peaks in intensity at the fault zone in association with either partitioned or oblique slip [*Fitzgerald et al*., 1993; *Tippett and Kamp*, 1993]. Analog experiments using clay cake and other materials similarly indicate that transpression is accommodated directly within strike-slip fault zones [*Wilcox et al*., 1973; *Odonne and Vialon*, 1983]. These observations are consistent with theoretical analyses of transpression and strain partitioning, which predict uplift within deformation belts adjacent to strike-slip faults, particularly within narrow deformation zones and along faults with obliquities to plate motion (α) of >20° [*Tikoff and Teyssier*, 1994; *Fossen and Tikoff*, 1998].

However, crustal deformation patterns can be misleading about the mechanisms of accommodating oblique plate motions. Geological indicators of vertical strain can be laterally advected along strike-slip zones, thereby juxtaposing deformation zones with foreign boundary conditions [*Anderson*,

1990; *Wakabayashi et al*., 2004]. Deformation may also be focused or distributed heterogeneously, due to the relatively rigid motion of upper crustal blocks in response to distributed motion in the lower lithosphere, such that patterns of brittle deformation may reflect the irregular transmission of strain via attachment zones rather than the general response of the lithosphere to oblique plate motion [*Bourne et al*., 1998; *Teyssier et al*., 2002]. For these reasons, case studies are needed to assess the contribution of local and regional structures and the timing of activity in response to transpressive deformation in the near-field along major fault zones.

The northern San Gabriel Mountains (NSGM) are located adjacent to the San Andreas fault (SAF) and are thought to have uplifted contemporaneously with the San Gabriel Mountains to the southeast due to oblique convergence along the Pacific-North America plate boundary (Figure 2.1) [*Dibblee*, 1982]. The range sits between the San Emigdio and San Gabriel Mountains along a highly oblique section of the SAF known as the "Big Bend" ($\alpha > 20°$), which spans ~300 km in southern California [*Hill and Dibblee*, 1953]. Given this magnitude of obliquity, the SAF along the NSGM should be experiencing pure-shear dominated transpression, which is favorable for near-field uplift [*Fossen and Tikoff*, 1998]. The rugged topography of the NSGM is consistent with near-field bedrock uplift and is similar to other areas in the Transverse Ranges where bedrock uplift has been identified close to the SAF. *Spotila et al*. [2001] suggested that elongate

ridges in the NSGM, including Portal Ridge (Figure 2.1), may be analogs to Yucaipa Ridge, a narrow crystalline sliver in the San Bernardino Mountains that has experienced Quaternary exhumation at ≥5 mm/yr in the near-field of the SAF. This rapid exhumation has occurred along the highly oblique Big Bend, but a secondary restraining bend at San Gorgonio Pass and intersecting faults, such as the Pinto Mountain fault and eastern California shear zone, complicate the kinematics and make it difficult to ascribe the rock uplift solely to overall obliquity of the southern SAF. By comparison, the NSGM lie along a simpler stretch of the SAF with no major intersecting structures or secondary restraining bends, such that it is in an ideal location to examine the links between oblique convergence and transpressive mountain building.

Although the complex geologic history of the NSGM during translation along the SAF has been studied [*Ehlig*, 1981; *Dibblee*, 1982; *Crowell*, 1982, 2003; *Meisling and Weldon, 1989; Matti and Morton*, 1993; *Powell*, 1993], the neotectonics and uplift history have not been explained or linked to modern transpression and are poorly understood relative to other areas along the SAF. We have used low-temperature thermochronometry and geomorphic observations to constrain the pattern and history of exhumation in association with transpressive plate motion along the NSGM. Results suggest the range has not experienced major near-field contraction due to modern transpressive deformation, but rather experienced short-lived block tilting related to the crossover from the San Gabriel

fault and activation of the modern trace of the SAF at ~5 Ma. This shows that contraction must be accommodated elsewhere in the SAF system, which is ~300 km wide in southern California. This also implies a heterogeneous crustal response to transpression and that local structural complexities are key for major near-field uplift along strike-slip faults.

Geologic Background

The NSGM consist of San Gabriel Mountain-type basement [*Matti and Morton*, 1993] and are isolated from other mountain blocks of the Transverse Ranges by structural lows (Figure 2.2). The primary structural high is the Clearwater block, a ~12-km-wide, lens-shaped wedge of Mesozoic granitic plutons interspersed within Precambrian gneiss. It is framed on the west by Ridge Basin across the Liebre fault, on the east-southeast by Soledad Canyon and the Sierra Pelona anticlinal ridge of Cretaceous-Paleocene Pelona Schist across the San Francisquito fault, on the south by the San Francisquito block across the Clearwater fault, and on the northeast by Portal Ridge and the Mojave basin across the SAF [*Jennings and Strand*, 1969; *Ehlig*, 1981; *Nourse*, 2002]. Ridge Basin is a deep (~14 km) transtensional basin that experienced active deposition from mid- to late-Miocene and exhibits subdued topography due to tectonic inversion since the Pliocene [*Crowell*, 1982, 2003]. Soledad Canyon is another structural low that filled with mainly non-marine sediment concurrently with

Ridge Basin prior to initiation of the San Gabriel fault [*Matti and Morton*, 1993]. The San Francisquito block is a ~6-km-wide wedge of Paleocene marine (San Francisquito Formation) and Oligocene non-marine strata (Vasquez Formation) located between the Clearwater and San Francisquito faults that narrows to the east [*Dibblee*, 1997]. Portal Ridge is an elongate sliver of Mesozoic granite and Pelona Schist that extends along the SAF, but disappears into the Mojave basin to the northeast.

Of all of the faults bounding the NSGM, only the Mojave segment of the SAF is known to be active, with ~35 mm/yr of right-slip motion [*Weldon and Sieh*, 1985; *Salyards et al*., 1992]. This is more than two-thirds of the relative motion between the Pacific and North American plates (~49 mm/yr), with modern motion of the Pacific plate directed to the northwest at an oblique angle to the SAF [~N36°W; *DeMets et al*., 1990]. Other structures associated with blocks of the NSGM reflect episodes of deformation during translation along the SAF since the mid-Miocene [*Crowell*, 1982; *Ehlig*, 1982; *Matti and Morton*, 1993; *Rust*, 1998]. The San Gabriel fault was the primary Pacific-North American plate boundary from 12-5 Ma and accumulated ~42-60 km of dextral slip before the SAF became active [*Ehlig*, 1981; *Crowell*, 1982; *Matti and Morton*, 1993; *Powell*, 1993; *Nourse*, 2002]. A shift in plate motion from the San Gabriel fault to the SAF at ~5 Ma resulted in termination of transtensional deposition in Ridge Basin and subsequent convergence due to slip transfer to the SAF [*Crowell*, 1982;

Ehlig, 1982; *Matti and Morton*, 1993; *Crowell*, 2003]. Secondary faults activated during this shift include the Clearwater, San Francisquito, and Liebre faults (Figure 2.2) [*Crowell*, 1982, 2003; *Powell*, 1993]. The Clearwater fault extends along the southern edge of the Clearwater block with a near-vertical dip and has experienced close to 5 km oblique dextral-reverse slip at 10-7.8 Ma [*Stanley*, 1966; *Ensley and Verosub*, 1982; *Crowell*, 1982, 2003; *Link*, 1983; *Fuis et al*., 2003; *Yan et al*., 2005]. The San Francisquito fault defines the southern boundary of the San Francisquito and eastern Clearwater blocks and exhibits ~3 km dextral slip and minor dip slip in the field [*Konigsberg*, 1967], but is believed to have accommodated ~110 km dextral slip at 22-13 Ma as a strand of the proto-San Andreas fault [*Powell*, 1993]. The Liebre fault extends along the southern flank of Liebre Mountain and was active at 7.3-6 Ma with oblique dextral-reverse slip of close to 10 km [*Faggioli*, 1952; *Ensley and Verosub*, 1982; *Crowell*, 1982, 2003; *Link*, 1983]. This fault may be an extension of the Squaw Peak-Santa Ana thrust of the western San Bernardino Mountains, corresponding to post-Miocene displacement on the SAF of 160 km [*Frizzell et al*., 1986; *Meisling and Weldon*, 1989].

The timing and kinematics of uplift of NSGM topography are not constrained. *Blythe et al*. [2000] analyzed the cooling histories and topographic development of the western San Gabriel Mountains southeast of Soledad Canyon, but did not extend the study to the NSGM (Figure 2.1). Although secondary

convergent structures are thought to be inactive, the range may have been built recently due to deep thrusts that daylight farther south. Seismic images from both transects of the Los Angeles Regional Seismic Experiment (LARSE) across the San Gabriel Mountains and NSGM reveal major reflectors that are interpreted to be thrust faults that extend below the southern front of the Transverse Ranges to join a décollement that intersects the San Andreas fault at a depth of ~22 km (transect locations shown in Figure 2.1) [*Fuis et al*., 2001, 2003]. Wholesale uplift of this crustal wedge above the inferred mountain-front thrusts may be responsible for uplift and exhumation of the NSGM or the range may reflect recent transpressive uplift on the SAF on unknown structures, but these hypotheses are not yet constrained by data.

Geomorphology of the NSGM

The topography of mountain belts reflects tectonic history, climate, and geomorphic boundary conditions. Coarse topographic traits, such as distributions of elevation and slope and drainage networks, can be the basis for simple inferences about uplift and erosion history. To analyze the role of structures on NSGM uplift, we examined topography using 30 m digital elevation models.

Elevation and relief reflect the relative impact of surface uplift and incision. Although the NSGM have rugged topography, peak elevations are ~1.5 km lower than those reached in similar bedrock elsewhere in the central

Transverse Ranges (Table 2.1). This suggests that either less surface uplift and/or more erosional downwearing has occurred. The Clearwater block has the most prominent topography in the NSGM. To the northwest, elevation increases to a maximum at Burnt Peak (1764 m), although relief is subdued across Liebre Mountain (Figures 2.3-2.4). To the southeast, mean elevation decreases, but local ridges and peaks, such as Jupiter Mountain, maintain overall relief and make the topography seem more rugged than to the west (Figures 2.3-2.4, Table 2.1). This may be a function of variable lithology in these areas, although both ends of the Clearwater block are dominated by Mesozoic granite. To the west, Ridge Basin has the lowest elevation in the NSGM (Table 2.1), but has a high frequency of short peaks and comparable relief that is consistent with erodible stratigraphy and basin inversion since transtensional deposition [*Crowell*, 1982, 2003; *Weldon et al*., 1993]. The lowest maximum elevation and relief occur at Portal Ridge.

Topographic slope is a loose proxy for denudation rate and/or tectonic activity in orogens [*Spotila et al*., 2002]. The highest average slope in the NSGM occurs in the central Clearwater block southwest of Burnt Peak (Figure 2.3a, Table 2.1), where topography appears as rugged as rapidly eroding areas of the San Gabriel Mountains to the east [*Blythe et al*., 2000; *Spotila et al*., 2002]. This could represent a locus of tectonic uplift or may be the result of relatively high precipitation focused in this area (Figure 2.3c). However, the lack of a correlation between precipitation and slope in the eastern part of Liebre Mountain and the

dense array of faults in the central Clearwater block suggest that other factors complicate topographic slope. In contrast, patches of relatively low slope characterize other areas in the NSGM. Liebre and Sawmill Mountains are both topped by low-slope erosional surfaces bounded by steep flanks (Figures 2.3a and 2.4). These appear comparable in the field to weathered surfaces developed in similar granitic bedrock in the San Bernardino Mountains, which have been inferred to be structural markers of minimal syn-tectonic denudation [*Spotila and Sieh*, 2000]. To the southeast, bands of gentle slope in the Clearwater block represent wide valleys separating isolated ridges and peaks with steeper slopes (Figure 2.3). If the erosional surface atop Liebre Mountain once projected eastward, then these wide valleys may reflect deep incision below a paleosurface that subsequently filled with sediment. Slope in Ridge Basin is the lowest for the area south of the SAF, possibly reflecting the presence of a more easily erodible lithology. To the north, Portal Ridge has similar erosional surfaces and the lowest average slope in the NSGM, suggesting minimal recent denudation (Figure 2.3a, Table 2.1).

Examination of the fluvial geomorphology of the range shows that the dominant drainage structure in the NSGM consists of streams flowing to the southwest, with a prominent divide alongside the SAF separating Mojave-draining rivers to the north (Figure 2.3d). Liebre Mountain controls drainage in the northwestern part of the NSGM (Fish Canyon), but the central (Elizabeth

Lake Canyon) and eastern (Leona Valley) stream networks drain the SAF valley to the southwest and northeast, respectively, suggesting that factors other than near-field uplift control drainage development.

Although these coarse topographic characteristics offer clues about the recent uplift activity of the NSGM, it is important to note that other boundary conditions such as erodibility, vegetation, and precipitation also affect topographic development. The NSGM are environmentally similar to the San Gabriel Mountains to the east, where erosion is heavily influenced by the cycle of wildfires in dry chaparral vegetative cover and the subsequent occurrence of large precipitation events during wet winters [*Lavé and Burbank*, 2004]. In the NSGM, which are more heavily vegetated and susceptible to wildfires along southern slopes and experience greater precipitation to the south, erosion is expected to be faster on the southern windward flank of the range. Some topographic and geomorphic characteristics, such as the steep slopes of Elizabeth Lake Canyon, may thus be an artifact of environmental rather than tectonic or lithologic influences.

Low-temperature thermochronometry in the NSGM

Methods

To examine the near field effect of pure-shear dominated transpression on a major continental strike-slip fault [*Tikoff and Teyssier*, 1994], we used low-temperature thermochronometry to establish the pattern of recent bedrock exhumation along the SAF in the NSGM. Samples from the NSGM were analyzed using apatite (U-Th)/He dating. This technique is a low-temperature thermochronometer with a typical closure temperature of ~60-80°C that varies with grain size and cooling rate [*Wolf et al*., 1996; *Farley*, 2000; *Ehlers and Farley*, 2003]. Model apatite cooling ages (AHe) can be interpreted as the time rocks cooled through these low closure temperatures, or exhumed through upper-crustal depths of ~2-3 km, depending on the geothermal gradient. Although crustal temperature gradients can affect cooling ages, the central part of the NSGM exhibits little variation in heat flow (65-72 mW/m^2) for sites up to 7 km from the SAF trace and is within range of the mean heat flow for the entire Mojave segment of the SAF (66 mW/m^2) that includes data 60 km from the fault [*Lachenbruch and Sass*, 1980].

To evaluate the pattern of exhumation associated with the SAF, rocks were collected along Portal Ridge and throughout the Clearwater and San Francisquito blocks. Sampling was focused on both sides of the SAF and along

the Clearwater and San Francisquito faults to establish how activity along these structures contributes to block exhumation. Rocks collected along vertical transects at Burnt Peak and Jupiter Mountain were used to constrain the exhumational history at each end of the Clearwater block. However, the rugged terrain, poor access, and minimal range in elevation limited the areal and vertical extent of sampling.

Ages were measured using the (U-Th)/He dating laboratory at Virginia Tech. Samples consisting of 1-7 apatite grains were outgassed in a resistance furnace at 940°C for 20 minutes and analyzed for ^{4}He by ^{3}He spike and quadrupole mass spectrometry. Radiogenic parent isotopes were measured by isotope dilution and ICP mass spectrometry at Yale University. Analytical uncertainties associated with measurement of ^{4}He, U, and Th, and alpha ejection correction factor (based on grain size and shape) amount to ±10% (2σ), which matches the typical reproducibility on natural samples and known standards. Reproducibility for ages measured in this study is generally better; the average standard deviation for eight well-reproduced samples run in triplicate is ±1.8% (Table 2.2). A subset of six samples was dated at the Noble Gas Laboratory at Caltech. Helium outgassing on these was accomplished via a Nd-YAG laser, but all other procedures were similar. Uncertainties in these ages are ±6% (2σ) [*Farley*, 2002]. Cross calibration between Caltech and Virginia Tech was accomplished by measuring multiple aliquots of Durango fluorapatite standard.

The average Durango age obtained at Caltech [32.1±1.7 Ma (1σ); n = 11; *House et al*., 2000] and Virginia Tech [30.9±1.53 Ma (1σ), n=40] is overlapping and consistent with the known cooling age of this volcanic sample [31.44±0.18 Ma (2σ); *McDowell et al*., 2005], thus verifying consistency between laboratories. An observation worth mentioning is the good reproducibility in age determinations despite relatively poor sample quality. Most apatites large enough to produce sufficient ^{4}He with low alpha ejection corrections contained conspicuous, low-birefringent inclusions, yet yielded reproducible ages. Overall we observed a poor correlation between age reproducibility and the presence of minor, low-birefringent inclusions, which indicates that large, easy to pick apatite of moderate quality should not be overlooked during grain selection for (U-Th)/He analysis.

Observations and Interpretations

Measured ages are pre-Pliocene and bear no clear spatial relationship to the SAF (Figure 2.5, Table 2.2). All ages are younger than the oldest AHe ages (~65 Ma; i.e. Laramide) typically observed in the Transverse Ranges and the Sierra Nevada [*Spotila et al*., 1998; *House et al*., 1998; *Blythe et al*., 2000]. If the NSGM bedrock experienced a similar exhumational history during and since the Cretaceous, then denudation has stripped away the upper kilometer or more of rocks containing isochrons of Laramide cooling ages. However, the youngest

AHe ages in the NSGM (4 Ma) are older than ages in areas of inferred recent, rapid exhumation, such as Yucaipa Ridge in the San Bernardino Mountains or the Thunder Peak block in the San Gabriel Mountains (~1-2 Ma) [*Spotila et al.*, 2001; *Blythe et al.*, 2002].

The pattern of ages in the NSGM is also uncommon for transpressive zones along the SAF. Unlike other areas [*Spotila et al.*, in press], cooling ages in the southern part of the NSGM do not decrease towards the fault (Figures 2.5 and 2.6a). Although the entire Clearwater block is within the near field of the SAF (i.e. within 10-20 km of the fault trace), the majority of these ages fail to imply recent, rapid denudation associated with transpressive rock uplift. The >10 Ma ages from the Portal Ridge block are particularly significant because they show that this crustal sliver is not exhuming rapidly from within the SAF zone. Ages from this block decrease towards the SAF, but imply exhumation occurred before local SAF initiation at ~5 Ma or that isochrons of a partial retention zone tilted in response to minor uplift (~500 m relief) along the SAF. These findings disprove the prediction of *Spotila et al.* [2001] that crustal exhumation history in the NSGM is similar to Yucaipa Ridge due to proximity to the oblique SAF.

The areal distribution of ages south of the SAF indicates a pattern that may relate to differential exhumation or block tilting. Cooling ages are clustered into young and old age groups at opposing ends of the Clearwater block, where ages are 4-5 Ma in the southeast and 8-33 Ma in the northwest (Figure 2.5). In

profile, the youngest ages (4-5 Ma) are found closest to the Clearwater-San Francisquito fault in the bottom section of the hanging wall, with ages increasing up-section to the northwest (Figure 2.6b). This asymmetrical age distribution contrasts with the minimal along-strike change in elevation, suggesting the block experienced tilting up to the east-southeast that is reflected in differential denudation and cooling. However, this pattern is not uniform, as locally ages differ from this trend (e.g., 8-11 Ma in eastern Liebre Mountain). The grouping of young ages along the eastern Clearwater-San Francisquito and Liebre faults suggests that this local variation may represent imbricate faulting or other local structure that has deformed isochrons. Moderately young ages (7.9 and 8.9 Ma) south of the Clearwater fault also suggest that the San Francisquito block exhumed with the Clearwater block in a shingled pattern top up to the east-southeast. Broad tilting of the Clearwater block is consistent with the presence of an erosional surface in the northwest. What is unclear, however, is when tilting occurred. The age pattern may reflect differential exhumation of samples through closure temperatures (i.e. deformation at ~5 Ma) or could represent deformation of pre-existing isochrons. Insight on timing of this deformation can be obtained from age-elevation relationships from Burnt Peak and Jupiter Mountain (Figure 2.6c). These represent the best vertical transects in the area (maximum relief and minimum lateral extent), although the total relief of both is small (~600-800 m). At Jupiter Mountain, ages are nearly invariant with elevation over ~350 m of

relief, implying rapid cooling at ~5 Ma. This may indicate that differential rock uplift and tilting were coeval with sample closure in the late Miocene. In contrast, the age-elevation gradient between two closely spaced samples at Burnt Peak show ~10 Ma difference over comparable relief, suggesting that cooling was slower than that to the southeast or that this area preserves a He partial retention zone (i.e. minimal exhumation).

Discussion

Modern Transpression

Thermochronometry and basic topographic form provide the first constraints on the kinematics of block uplift and exhumation in the NSGM. Exhumation rates in the NSGM are considerably slower than in other areas along the Big Bend section of the SAF [*Spotila et al.*, 2001]. We estimated exhumation rates for individual AHe ages using the iterative method for closure temperature of *Dodson* [1973] and a static one-dimensional geothermal gradient. Closure temperature for each sample was calculated using assumed parameters of activation energy (33000 cal/mol) and diffusivity at infinite temperature (50 cm^2/s), the individual grain shape and size, and approximate cooling rate based on iterative calculation from closure temperature and sample age [*Dodson*, 1973; *McDougall and Harrison*, 1988; *Farley*, 2000]. AHe ages were then converted to

exhumation rates using an assumed geothermal gradient of 30°C/km [*Lachenbruch et al.*, 1985] and an ambient surface temperature of 10°C. Assuming closure isotherms are roughly parallel to local mean elevation and given that samples were collected from approximately mean elevation at each location, exhumation rates were not adjusted for local sample elevation. The resulting maximum exhumation rates are 0.4 mm/yr for Jupiter Mountain (JBSG5), 0.2 mm/yr for Portal Ridge (LL5), and <0.1 mm/yr for Burnt Peak (JBSG7). These rates could be uncertain to ±50%, given potential variations in geothermal gradient or isotherm shape. Regardless, these rates are an order of magnitude lower than the rapid rates of 5-7 mm/yr estimated for Yucaipa Ridge along the southern SAF [*Spotila et al.*, 2001]. The lack of clear evidence for recent, rapid exhumation in the near field of the SAF implies the crustal response to transpression along the Big Bend is heterogeneous. The possibility of differential exhumation and tilting of the Clearwater block, in contrast, suggests a deformation event that may have been related to an earlier stage of the plate boundary's history. Both of these results have implications for our understanding of transpression.

Although near-field uplift is commonly associated with transpressive deformation along faults [e.g., *Wilcox et al.,* 1973; *Sylvester*, 1988; *Fossen and Tikoff*, 1998; *Spotila et al*., 2001], our results do not require major rock uplift in the past few Ma in the NSGM. Despite the presence of mountainous topography

in this area, we propose based on AHe ages that the deformation that built the range was earlier. Yet, the SAF is >20° oblique to plate motion along the NSGM and should be experiencing pure-shear dominated transpression [*Tikoff and Teyssier*, 1994] as seen in the San Gabriel and San Bernardino Mountains [*Spotila et al*., 1998, 2001; *Blythe et al*., 2000]. This implies a heterogeneous crustal response to transpression, whereby crustal blocks replete with preexisting faults may lie directly within transpressive zones and not deform continuously. This may further suggest that other cases of near-field SAF uplift, such as Yucaipa Ridge, may be partially dependent on local structural complexities, such as the restraining bend at San Gorgonio Pass [*Spotila et al*., 2001]. Local complexity from secondary structures, such as intersecting conjugate faults [e.g., Pinto Mountain fault in San Bernardino Mountains and Garlock fault in San Emigdio Mountains; *Spotila et al*., 2001; *Niemi et al*., 2004], may thus contribute more to mountain building along major strike-slip faults than previously thought. This is consistent with GPS data for the Mojave segment of the SAF, where vectors are aligned parallel to the trace of the fault [*Argus et al*., 2005]. Large-scale shortening in the Los Angeles basin is also observed from GPS data [*Argus et al*., 1999], which may be related to far-field activity on thrust faults that connect to the SAF and suggest that high obliquity is partitioned across a wide, diffuse zone. Large block rotations may also redistribute compression by deflecting convergence [*Terres and Luyendyk*, 1985; *Golombek and Brown*, 1988].

Earlier Transpressive Deformation

Given the possibility that tilting of the Clearwater block occurred in the late Miocene, it is important to consider the location and tectonic setting of the block at the time this deformation occurred. The Clearwater block restores along the SAF to ~160 km to the southeast between the San Gabriel and San Bernardino Mountains at ~7 Ma (Figure 2.7a) [*Frizzell et al*., 1986; *Matti and Morton*, 1993; *Powell*, 1993]. At ~5 Ma, motion along the San Gabriel fault stepped northeast across the Clearwater block to the modern trace of the SAF [*Matti and Morton*, 1993], approximately concurrent with an abrupt ~5° clockwise rotation of Pacific plate motion (Figure 2.7b) [*Cox and Engebretson*, 1985; *Atwater and Stock*, 1998]. This change in plate motion may have induced a change in San Gabriel and Mojave block motion from clockwise to counterclockwise rotation [*Terres and Luyendyk*, 1985; *Golombek and Brown*, 1988]. During the stepover from the San Gabriel fault to the modern SAF, the Clearwater-San Francisquito and Liebre faults may have been activated as intermediary plate boundary faults, based on intersections of these faults with the SAF and the timing of activity (Figure 2.7b) [*Powell*, 1993; *Yan et al*., 2005]. *Meisling and Weldon* [1989] propose that the Liebre fault was part of a larger fault system (Squaw Peak-Liebre Mountain fault) that thrust the proto-San Bernardino Mountains to the southwest over the Clearwater block between 9.5 to 4 Ma (Figure 2.7b). It is possible that a transitional restraining bend that included this Squaw Peak-Liebre Mountain

thrust induced tilting and exhumation of the Clearwater block at ~4-5 Ma as the modern trace of the SAF became established (Figure 2.7c). This shortening may have also facilitated compressional downflexing of Ridge Basin, which is supported by post-Pliocene activation of faults and folds that extend parallel to and between the Clearwater and Liebre faults [*Crowell*, 1982, 2003; *Weldon et al*., 1993]. Therefore, the Clearwater block tilting may be related to downflexing along the Squaw Peak-Liebre Mountain fault in the west and rapid uplift of the narrowing Clearwater block to the southeast. We speculate that this deformation event was short-lived, with subsequent lateral translation of a relatively rigid Clearwater block along the modern trace of the SAF over the last ~5 Ma (Figure 2.7d).

Other crustal block histories in the region may be similar to our speculative scenario for the Clearwater block. The Circle-Table Mountain crustal sliver in the northern part of the San Gabriel Mountains may have experienced a fault crossover in the mid-Miocene and translation through a restraining bend and exhibits a similar along-strike decrease in AHe and apatite fission track ages to the southeast as the Clearwater block [*Matti and Morton*, 1993; *Blythe et al*., 2002]. A similar fault crossover from the Banning fault northeast across the Morongo block to the Punchbowl-Wilson Creek strand of the SAF occurred at ~5 Ma, resulting in rapid exhumation of the Morongo block in the San Bernardino Mountains [*Blythe et al*., 2002]. These microblock pop-ups may be recorders of

transitional tectonic settings, because of the narrow width and lack of connectivity to the SAF or other major faults. Larger crustal blocks, such as the San Gabriel Mountains, appear to have a more established connection between mountain-front thrusts and the SAF [*Fuis et al*., 2001, 2003], requiring larger structures and events to cause whole-block exhumation.

Implications for Transpression

Our hypothesis that uplift and deformation of the NSGM occurred in response to a local fault crossover as the modern SAF became established is consistent with a view that the crustal response to transpression is heterogeneous and that local structural complexity facilitates transpressive deformation (Figure 2.8). Major strike-slip faults such as the SAF are typically wide zones that accommodate large displacement via an array of evolving strands. These fault zones are complex areas of slip transfer and fault junctions, where two crustal plates slide along an irregular interface that can wedge crustal slivers to create local transpression. Slight changes in the main fault geometry associated with intersecting structures, vertical axis rotations of adjacent crust, and other factors can easily lead to significant local convergent or divergent deformation, given that only a small fraction of the horizontal velocity needs to be transformed into secondary pure shear deformation to have a major geologic and geomorphic impact. For example, *Meisling and Weldon* [1989] explained local uplift in the

northern part of the San Gabriel Mountains as a migrating anticline, the western San Bernardino arch, which may be caused by a small subsurface welt on the SAF due to its confluence with the San Jacinto fault. Local deformation due to the crossover from the San Gabriel fault to the SAF would represent a similar local event, rather than wholesale transpressive deformation on the SAF due to the obliquity of the Big Bend.

If the NSGM were produced by local structural complexity in an earlier stage of the SAF's history, it raises the question as to why wholesale pure-shear deformation, as predicted by models of tranpressive deformation for the lower crust [*Tikoff and Teyssier*, 1994; *Fossen and Tikoff*, 1998], is not more readily apparent along the Big Bend. Wholesale transpressive deformation does occur along the Alpine fault in New Zealand, a strike-slip plate boundary with comparable obliquity and slip rate as the Big Bend [*Tippett and Kamp*, 1993; *Teyssier et al*., 1995; *Braun and Beaumont*, 1995]. The reason for the difference in deformation styles despite similar boundary conditions at these two plate boundaries is not known. However, it is possible that minor transpressive deformation and uplift occurs along the NSGM in the present day, despite the likelihood that cooling ages reflect early deformation. North-south directed compression that is concentrated along the San Gabriel Mountain range front to the southeast [*Argus et al*., 1999] might also produce minor uplift of the NSGM. Future geomorphic studies may reveal whether minor uplift occurs today within

the NSGM. Still, the lack of major pure shear deformation in the near field in the NSGM implies the major obliquity to plate motion must be accommodated farther from the transpressive zone of the SAF, perhaps by the western Transverse Ranges or by vertical axis rotation to the east and west. It also implies caution is needed when relating crustal deformation to specific structures or plate boundary conditions. Although it is tempting to attribute all of the central Transverse Ranges mountain building as near-field pure shear deformation due to the Big Bend, our case study indicates a more complex history. This illustrates the value of local case studies in the analysis of continental deformation systems.

Conclusions

Low-temperature cooling ages from the NSGM are older than those from other blocks along the Big Bend of the southern SAF, where rapid exhumation is inferred in the last few million years. There is no decrease in AHe ages towards the SAF in the Clearwater block, implying that major bedrock uplift and associated exhumation is not currently occurring along the fault zone or within the near field. Instead, there is an along-strike variation in age and topographic character that seems to reflect block tilting subparallel to the trace of the SAF. Based on restored block locations and the timing of fault activity, we propose that this tilting event was created by the slip transfer of the San Gabriel fault to the SAF at ~5 Ma, although the exact mechanism is not clear. Thus, despite plate

motion being >20° oblique along the southern SAF, implying pure-shear dominated conditions along this fault stretch, there appears to be no major modern near-field shortening in the NSGM. This suggests that the crustal response to transpression is heterogeneous and that shortening is accommodated farther away from the fault trace. We speculate that near-field uplift of other areas along the southern SAF may actually reflect local structural complexities instead of the regional obliquity to plate motion. This illustrates the importance of detailed case studies that examine the actual mechanisms of transpression, beyond the understanding provided by the general distribution of rugged topography and exhumation rate along major faults.

References

Anderson, R.S. (1990), Evolution of the northern Santa Cruz Mountains by advection of crust past a San Andreas fault bend, *Science*, *249*, 397-401.

Argus, D.F., M.B. Heflin, A. Donnellan, F.H. Webb, D. Dong, K.J. Hurst, D.C. Jefferson, G.A. Lyzenga, M.M. Watkins, and J.F. Zumberge (1999), Shortening and thickening of metropolitan Los Angeles measured and inferred by using geodesy, *Geology*, *27*, 703-706.

Argus, D.F., M.B. Heflin, G. Peltzer, F. Crampé, and F.H. Webb (2005), Interseismic strain accumulation and anthropogenic motion in metropolitan Los Angeles, *J. Geophys. Res.*, *110*, B04401, doi:10.1029/2003JB002934.

Atwater, T. and J. Stock (1998), Pacific-North America plate tectonics of the Neogene southwestern United States: An update, *Int. Geol. Rev.*, *40*, 375-402.

Blythe, A.E., D.W. Burbank, K.A. Farley, and E.J. Fielding (2000), Structural and topographic evolution of the central Transverse Ranges, California, from apatite fission-track, (U-Th)/He and digital elevation model analyses, *Basin Res.*, *12*, 97-114.

Blythe, A.E., M.A. House, and J.A. Spotila (2002), Low-temperature thermochronology of the San Gabriel and San Bernardino Mountains, southern California: Constraining structural evolution, in *Contributions to Crustal Evolution of the Southwestern United States: Boulder, Colorado*, edited by A. Barth, *Geol. Soc. Am. Spec. Pap.*, *365*, 231-250.

Bourne, S.J., P.C. England, and B. Parsons (1998), The motion of crustal blocks driven by flow of the lower lithosphere and implications for slip rates of continental strike-slip faults, *Nature*, *391*, 655-659.

Braun, J. and C. Beaumont (1995), Three-dimensional numerical experiments of strain partitioning at oblique plate boundaries: Implications for contrasting tectonic styles in the southern Coast Ranges, California, and central South Island, New Zealand, *J. Geophys. Res.*, *100*, 18,059-18,074.

Bürgmann, R. (1991), Transpression along the southern San Andreas fault, Durmid Hill, California, *Tectonics*, *10*, 1152-1163.

California Division of Mines and Geology, [CD-ROM 2000-007 (2000)], GIS Data for the Geologic Map of California.

Cox, A. and D.C. Engebretson (1985), Change in motion of Pacific plate at 5 Myr BP, *Nature*, *313*, 472-474.

Crowell, J.C. (1982), The tectonics of Ridge Basin, southern California, in *Geologic History of Ridge Basin, Southern California*, edited by J.C.

Crowell and M.H. Link, Pacific Section, Society of Economic Paleontologists and Mineralogists, Los Angeles, California, 25-42.

Crowell, J.C. (2003), Tectonics of Ridge Basin region, southern California, in *Evolution of Ridge Basin, Southern California: An Interplay of Sedimentation and Tectonics*, edited by J.C. Crowell, *Geol. Soc. Am. Spec. Pap.*, *367*, 157-203.

DeMets, C., R.G. Gordon, D.F. Argus, and S. Stein (1990), Current plate motions, *Geophys. J. Int.*, *101*, 425-478.

Dibblee, T.W., Jr. (1982), Geology of the Castaic Block, the mountains and hills northwest of the San Gabriel Mountains, southern California, in *Geology and Mineral Wealth of the California Transverse Ranges*, edited by D.L. Fife and J.A. Minch, Mason Hill Volume, Santa Ana, California, South Coast Geological Society Guidebook 10, 78-93.

Dibblee, T.W., Jr. (1997), Geologic map of the Warm Springs Mountain quadrangle, Los Angeles County, California, Dibblee Geological Foundation Map DF-64, edited by H.E. Ehrenspeck, 1:24000.

Dodson, M.H. (1973), Closure temperature in cooling geochronological and petrological systems, *Contrib. Mineral. Petrol.*, *40*, 259-274.

Ehlers, T.A. and K.A. Farley (2003), Apatite (U-Th)/He thermochronometry: Methods and applications to problems in tectonic and surface processes, *Earth Planet. Sci. Lett.*, *206*, 1-14.

Ehlig, P.L. (1981), Origin and tectonic history of the basement terrane of the San Gabriel Mountains, central Transverse Ranges, in *The Geotectonic Development of California*, *Rubey Volume I*, edited by W.G. Ernst, Prentice-Hall, Englewood Cliffs, New Jersey, 253-283.

Ehlig, P.L. (1982), The Vincent thrust: Its nature, paleogeographic reconstruction across the San Andreas fault, and bearing on the evolution of the Transverse Ranges, in *Geology and Mineral Wealth of the California Transverse Ranges*, edited by D.L. Fife and J.A. Minch, Mason Hill Volume, Santa Ana, California, South Coast Geological Society Guidebook 10, 370-379.

England, P.C. and G. Houseman (1985), Role of lithospheric strength heterogeneities in the tectonics of Tibet and neighbouring regions, *Nature*, *315*, 297-301.

Ensley, R.A. and K.L. Verosub (1982), A magnetostratigraphic study of the sediments of the Ridge Basin, southern California and its tectonic and sedimentological implications, *Earth Planet. Sci. Lett.*, *59*, 192-207.

Faggioli, R.E. (1952), The geology of the Liebre fault, M.A. thesis, 56 pp., Univ. of Calif. at Los Angeles, Los Angeles, Calif.

Farley, K.A. (2000), Helium diffusion from apatite: General behavior as illustrated by Durango fluorapatite, *J. Geophys. Res.*, *105*, 2903-2914.

Farley, K.A. (2002), (U-Th)/He dating: Techniques, calibrations, and applications, *Rev. Mineral. Geochem.*, *47*, 819-843.

Fitzgerald, P.G., E. Stump, and T.F. Redfield (1993), Late Cenozoic uplift of Denali and its relation to relative plate motion and fault morphology, *Science*, *259*, 497-499.

Fossen, H. and B. Tikoff (1998), Extended models of transpression and transtension, and application to tectonic setting, *Geol. Soc. Spec. Publ.*, *135*, 15-33.

Foster, D.A., A.J.W. Gleadow, and G. Mortimer (1994), Rapid Pliocene exhumation in the Karakoram (Pakistan), revealed by fission-track thermochronology of the K2 gneiss, *Geology*, *22*, 19-22.

Frizzell, V.A., Jr., J.M. Mattinson, and J.C. Matti (1986), Distinctive Triassic megaporphyritic monzogranite: Evidence for only 160 km offset along the San Andreas fault, southern California, *J. Geophys. Res.*, *91*, 14,080-14,088.

Fuis, G.S., T. Ryberg, N.J. Godfrey, D.A. Okaya, and J.M. Murphy (2001), Crustal structure and tectonics from the Los Angeles Basin to the Mojave Desert, southern California, *Geology*, *29*, 15-18.

Fuis, G.S., R.W. Clayton, P.M. Davis, T. Ryberg, W.J. Lutter, D.A. Okaya, E. Hauksson, C. Prodehl, J.M. Murphy, M.L. Benthien, S.A. Baher, M.D. Kohler, K. Thygesen, G. Simila, and G.R. Keller (2003), Fault systems of the 1971 San Fernando and 1994 Northridge earthquakes, southern California: Relocated aftershocks and seismic images from LARSE II, *Geology*, *31*, 171-174.

Golombek, M.P. and L.L. Brown (1988), Clockwise rotation of the western Mojave Desert, *Geology*, *16*, 126-130.

Hill, M.L. and T.W. Dibblee, Jr. (1953), San Andreas, Garlock, and Big Pine faults, California: A study of the character, history, and tectonic significance of their displacements, *Geol. Soc. Am. Bull.*, *64*, 443-458.

House, M.A., B.P. Wernicke, and K.A. Farley (1998), Dating topography of the Sierra Nevada, California, using apatite (U-Th)/He ages, *Nature*, *396*, 66-69.

House, M.A., K.A. Farley, and D. Stockli (2000), Helium chronometry of apatite and titanite using Nd-YAG laser heating, *Earth Planet. Sci. Lett.*, *183*, 365-368.

Jennings, C.W. and R.G. Strand (1969), Geologic map of California, Los Angeles sheet, Olaf P. Jenkins edition, California Division of Mines and Geology, 1:250000.

Konigsberg, R.L. (1967), Geology along the San Francisquito fault, Los Angeles County, California, M.S. thesis, 84 pp., Univ. of Calif. at Los Angeles, Los Angeles, Calif.

Lachenbruch, A.H. and J.H. Sass (1980), Heat flow and energetics of the San Andreas fault zone, *J. Geophys. Res.*, *85*, 6185-6223.

Lachenbruch, A.H., J.H. Sass, and S.P. Galanis, Jr. (1985), Heat flow in southernmost California and the origin of the Salton Trough, *J. Geophys. Res., 90*, 6709-6736.

Lavé, J. and D. Burbank (2004), Denudation processes and rates in the Transverse Ranges, southern California: Erosional response of a transitional landscape to external and anthropogenic forcing, *J. Geophys. Res.*, *109*, F01006, doi:10.1029/2003JF000023.

Link, M.H. (1983), Sedimentation, tectonics, and offset of Miocene-Pliocene Ridge Basin, California, in *Tectonics and Sedimentation Along Faults of the San Andreas System*, edited by D.W. Andersen and M.J. Rymer, Pacific Section, Society of Economic Paleontologists and Mineralogists, Los Angeles, California, 17-32.

Matti, J.C. and D.M. Morton (1993), Paleogeographic evolution of the San Andreas fault in southern California: A reconstruction based on a new cross-fault correlation, in *The San Andreas Fault System: Displacement, Palinspastic Reconstruction, and Geologic Evolution*, edited by R.E. Powell, R.J. Weldon, II, and J.C. Matti, *Geol. Soc. Am. Mem., 178*, 107-159.

McDougall, I. and T.M. Harrison (1988), *Geochronology and Thermochronology by the $^{40}Ar/^{39}Ar$ Method*, Oxford University Press, New York, 212 pp.

McDowell, F.W., W.C. McIntosh, and K.A. Farley (2005), A precise ^{40}Ar-^{39}Ar reference age for the Durango apatite (U-Th)/He and fission-track dating standard, *Chem. Geol.*, *214*, doi:10.1016/j.chemgeo.2004.10.002, 249-263.

Meisling, K.E. and R.J. Weldon, II (1989), Late Cenozoic tectonics of the northwestern San Bernardino Mountains, southern California, *Geol. Soc. Am. Bull.*, *101*, 106-128.

Molnar, P. (1988), Continental tectonics in the aftermath of plate tectonics, *Nature*, *335*, 131-137.

Niemi, N.A., J.A. Spotila, and M.A. House (2004), Crustal exhumation in a transpressional setting, the San Emigdio Mountains, California, *Geol. Soc. Am. Abstr. Programs*, *36*, 24.

Nourse, J.A. (2002), Middle Miocene reconstruction of the central and eastern San Gabriel Mountains, southern California, with implications for evolution of the San Gabriel fault and Los Angeles basin, in *Contributions to Crustal Evolution of the Southwestern United States: Boulder, Colorado*, edited by A. Barth, *Geol. Soc. Am. Spec. Pap*. *365*, 161-185.

Odonne, F. and P. Vialon (1983), Analogue models of folds above a wrench fault, *Tectonophysics*, *99*, 31-46.

Powell, R.E. (1993), Balanced palinspastic reconstruction of pre-late Cenozoic paleogeology, southern California: Geologic and kinematic constraints on evolution of the San Andreas fault system, in *The San Andreas Fault System: Displacement, Palinspastic Reconstruction, and Geologic Evolution*, edited by R.E. Powell, R.J. Weldon, II, and J.C. Matti, *Geol. Soc. Am. Mem.*, *178*, 1-106.

Rust, D. (1998), Contractional and extensional structures in the transpressive 'Big Bend' of the San Andreas fault, southern California, in *Continental Transpressional and Transtensional Tectonics*, edited by R.E. Holdsworth, R.A. Strachan, and J.F. Dewey, *Geol. Soc. London Spec. Publ.*, *135*, 119-126.

Salyards, S.L., K.E. Sieh, and J.L. Kirschvink (1992), Paleomagnetic measurement of nonbrittle coseismic deformation across the San Andreas fault at Pallett Creek, *J. Geophys. Res.*, *97*, 12,457-12,470.

Spotila, J.A., K.A. Farley, and K. Sieh (1998), Uplift and erosion of the San Bernardino Mountains associated with transpression along the San Andreas fault, California, as constrained by radiogenic helium thermochronometry, *Tectonics*, *17*, 360-378.

Spotila, J.A. and K. Sieh (2000), Architecture of transpressional thrust faulting in the San Bernardino Mountains, southern California, from deformation of a deeply weathered surface, *Tectonics*, *19*, 589-615.

Spotila, J.A., K.A. Farley, J.D. Yule, and P.W. Reiners (2001), Near-field transpressive deformation along the San Andreas fault zone in southern California, based on exhumation constrained by (U-Th)/He dating, *J. Geophys. Res.*, *106*, 30,909-30,922.

Spotila, J.A., M.A. House, A.E. Blythe, N.A. Niemi, and G.C. Bank (2002), Controls on the erosion and geomorphic evolution of the San Bernardino and San Gabriel Mountains, southern California, in *Contributions to Crustal Evolution of the Southwestern United States: Boulder, Colorado*, edited by A. Barth, *Geol. Soc. Am. Spec. Pap.*, *365*, 205-230.

Stanley, K.O. (1966), The structural history of the Clearwater fault, northwestern Los Angeles County, California, M.A. thesis, 73 pp., Univ. of Calif. at Los Angeles, Los Angeles, Calif.

Sylvester, A.G. (1988), Strike-slip faults, *Geol. Soc. Am. Bull.*, *100*, 1666-1703.

Terres, R.R. and B.P. Luyendyk (1985), Neogene tectonic rotation of the San Gabriel region, California, suggested by paleomagnetic vectors, *J. Geophys. Res.*, *90*, 12,467-12,484.

Teyssier, C., B. Tikoff, and M. Markley (1995), Oblique plate motion and continental tectonics, *Geology*, *23*, 447-450.

Teyssier, C., B. Tikoff, and J. Weber (2002), Attachment between brittle and ductile crust at wrenching plate boundaries, *European Geosciences Union Stephan Mueller Special Publication Series*, *1*, 75-91.

Thomson, S.N. (2002), Late Cenozoic geomorphic and tectonic evolution of the Patagonian Andes between latitudes 42 degrees S and 46 degrees S: An appraisal based on fission-track results from the transpressional intra-arc Liquiñe-Ofqui fault zone, *Geol. Soc. Am. Bull.*, *114*, 1159-1173.

Tikoff, B. and C. Teyssier (1994), Strain modeling of displacement-field partitioning in transpression orogens, *J. Struct. Geol.*, *16*, 1575-1588.

Tippett, J.M. and P.J.J. Kamp (1993), Fission track analysis of the late Cenozoic vertical kinematics of continental Pacific crust, South Island, New Zealand, *J. Geophys. Res.*, *98*, 16,119-16,148.

Vauchez, A. and A. Nicolas (1991), Mountain building: Strike-parallel motion and mantle anisotropy, *Tectonophysics*, *185*, 183-201.

Wakabayashi, J., J.V. Hengesh, and T.L. Sawyer (2004), Four-dimensional transform fault processes: Progressive evolution of step-overs and bends, *Tectonophysics*, *392*, 279-301.

Weldon, R.J., II and K.E. Sieh (1985), Holocene rate of slip and tentative recurrence interval for large earthquakes on the San Andreas fault, Cajon Pass, southern California, *Geol. Soc. Am. Bull.*, *96*, 793-812.

Weldon, R.J., II, K.E. Meisling, and J. Alexander (1993), A speculative history of the San Andreas fault in the central Transverse Ranges, California, in *The San Andreas Fault System: Displacement, Palinspastic Reconstruction, and Geologic Evolution*, edited by R.E. Powell, R.J. Weldon, II, and J.C. Matti, *Geol. Soc. Am. Mem.*, *178*, 161-198.

Wilcox, R.E., T.P. Harding, and D.R. Seely (1973), Basic wrench tectonics, *AAPG Bull.*, *57*, 74-96.

Wolf, R.A., K.A. Farley, and L.T. Silver (1996), Helium diffusion and low-temperature thermochronometry of apatite, *Geochim. Cosmochim. Acta*, *60*, 4231-4240.

Yan, Z., R.W. Clayton, and J. Saleeby (2005), Seismic refraction evidence for steep faults cutting highly attenuated continental basement in the central Transverse Ranges, California, *Geophys. J. Int.*, *160*, 651-666.

Table 2.1: Topographic features of the northern San Gabriel Mountains

Area	Area (km^2)	Min. Elev. (m)	Max. Elev. (m)	Avg. Elev. (m)	Total Relief (m)	Avg. Slope (°)
Ridge Basin (1)	281	360	1440	954	1080	16.3
Clearwater Block (2, 3, & 4)	363	603	1764	1153	1161	20.6
Western half of block (2)	76	1017	1760	1376	743	18.0
Middle portion of block (3)	141	612	1764	1139	1152	23.4
Eastern half of block (4)	146	605	1405	1047	800	19.0
Portal Ridge (5)	139	841	1367	1074	526	13.9
San Francisquito block (6)	104	452	1223	785	771	22.1

Numbers in parentheses correspond to areas outlined in Figure 2.3a.

Topographic features from other blocks in the central Transverse Ranges

Area	Min. Elev. (m)	Max. Elev. (m)	Avg. Elev. (m)	Total Relief (m)	Avg. Slope (°)
San Gabriel Mountains	121	3070	1351	2949	25.9
San Bernardino Mountains	407	3506	1616	3099	17.4

Topographic data for the San Gabriel and San Bernardino Mountains from *Spotila et al.* [2002], based on 90 m digital elevation models.

Table 2.2: AHe data for the northern San Gabriel Mountains

Sample	Elevation (m)	Latitude, Longitude	Rock type	Mass (mg)	mwar (μm)	He (pmol)	U (ppm)	Th (ppm)	# grains	F_T	Corr. age (Ma)	Average age (Ma)
JBSG1-1	1230	34.5991°N, 118.3900°W	granite	0.0048	40.0	0.0031	19.0	47.6	4	0.71	5.7	
-2				0.0056	33.7	0.0028	14.7	48.7	6	0.65	5.6	**5.6±0.1**
-3				0.0053	40.4	0.0032	17.6	49.0	5	0.72	5.6	
JBSG2-1	1340	34.6062°N, 118.4121°W	granodiorite	0.0085	43.4	0.0043	14.0	49.7	5	0.71	5.2	
-2				0.0089	42.5	0.0048	14.5	57.4	5	0.69	5.2	**5.2**
-3				0.0101	51.4	0.0040	9.7	40.0	5	0.74	5.2	
JBSG5-1	1077	34.5907°N, 118.3303°W	granite	0.0056	37.2	0.0019	14.2	39.9	5	0.67	4.1	
-2				0.0065	41.6	0.0035	21.0	52.6	4	0.70	4.3	**4.2±0.1**
-3				0.0036	55.2	0.0012	14.2	31.3	1	0.75	4.0	
JBSG6-1	1464	34.6878°N, 118.5249°W	granite	0.0019	48.3	0.0028	30.5	20.5	1	0.70	11.3	
-2				0.0032	35.6	0.0018	11.0	12.1	4	0.65	12.2	**10.5±1.8**
-3				0.0013	36.8	0.0008	19.3	16.8	1	0.68	8.1	
JBSG7-1	1749	34.6826°N, 118.5758°W	gneiss	0.0061	38.6	0.0292	28.9	24.7	5	0.64	41.3	
-2				0.0078	42.3	0.0282	33.6	10.8	5	0.71	26.8	**32.8±6.2**
-3				0.0040	36.6	0.0143	31.8	12.8	4	0.64	30.4	
JBSG9-1	1362	34.6923°N, 118.6070°W	granite	0.0030	46.0	0.0028	9.7	29.0	1	0.75	*14.5*‡	
-2				0.0064	38.9	0.0045	15.5	37.6	5	0.69	7.8	**8.3**
-3				0.0019	36.8	0.0013	12.3	33.5	1	0.72	8.8	
JBSG10-1	1735	34.7020°N, 118.6144°W	granite	0.0048	66.7	0.0038	9.3	27.5	1	0.81	11.7	
-2				0.0121	49.1	0.0103	12.5	31.2	7	0.72	11.2	**11.6±0.3**
-3				0.0131	44.3	0.0125	13.1	33.9	7	0.72	11.9	
JBSG11-1	1257	34.6767°N, 118.5624°W	gneiss	0.0048	35.3	0.0137	27.6	15.4	5	0.64	27.3	
-2				0.0045	37.5	0.0037	11.3	2.1	4	0.66	20.3	**22.9±3.2**
-3				0.0052	39.2	0.0065	15.2	7.8	4	0.67	20.9	
JBSG13-1	608	34.6035°N, 118.5572°W	gneiss	0.0094	41.8	0.0171	46.9	2.0	6	0.71	10.4	
-2				0.0102	45.2	0.0189	46.4	1.9	6	0.72	10.5	**10.4±0.1**
-3				0.0073	45.5	0.0141	48.8	3.0	4	0.73	10.3	
JBSG14-1	630	34.6109°N, 118.5626°W	gneiss	0.0146	53.6	0.0103	21.6	21.0	5	0.75	6.7	
-2				0.0110	47.1	0.0073	18.5	20.3	5	0.72	7.6	**7.0±0.4**
-3				0.0059	55.2	0.0035	16.0	22.7	1	0.77	6.8	
JBSG15-1	1184	34.6480°N, 118.4181°W	gneiss	0.0050	40.4	0.0069	41.2	23.2	4	0.69	8.1	
-2				0.0040	35.8	0.0086	57.3	40.1	4	0.63	9.8	**8.4±1.0**
-3				0.0069	45.0	0.0054	24.1	19.6	4	0.72	7.3	

Sample	Elevation (m)	Latitude, Longitude	Rock type	Mass (mg)	mwar (μm)	He (pmol)	U (ppm)	Th (ppm)	# grains	F_T	Corr. age (Ma)	Average age (Ma)
JBSG16-1	1099	34.6961°N, 118.6665°W	granodiorite	0.0062	38.7	0.0121	22.9	27.9	4	0.69	18.4	
-2				0.0099	42.5	0.0175	20.6	25.2	6	0.72	17.7	**18.1**
-3				0.0056	57.5	0.0017	21.3	31.3	1	0.80	*2.6* ‡	
JBSG18-1	1098	34.7183°N, 118.5312°W	granodiorite	0.0086	42.2	0.0188	29.4	17.1	5	0.70	17.8	
-2				0.0086	42.0	0.0190	31.4	33.2	5	0.72	15.0	**17.4±1.8**
-3				0.0099	45.3	0.0245	28.0	26.5	5	0.72	19.3	
JBSG20-1	1021	34.7201°N, 118.5111°W	granodiorite	0.0132	45.5	0.0164	12.3	20.6	6	0.72	19.1	
-2				0.0091	43.4	0.0157	19.0	30.4	5	0.72	17.5	**19.2±1.4**
-3				0.0138	52.0	0.0502	31.6	51.2	5	0.75	21.0	
JBSG21-1	1207	34.7180°N, 118.4905°W	granite	0.0092	43.9	0.0350	33.6	25.6	5	0.71	25.6	
-2				0.0072	39.8	0.0256	28.2	20.6	5	0.71	29.2	**26.9±1.6**
-3				0.0085	40.6	0.0238	24.9	18.7	5	0.70	26.0	
JBSG22-1	913	34.6958°N, 118.4013°W	granite	0.0086	42.6	0.0433	44.9	47.0	5	0.71	24.2	
-2				0.0088	41.3	0.0303	32.6	30.7	5	0.70	23.6	**23.4±0.7**
-3				0.0148	45.5	0.0559	35.1	35.4	6	0.74	22.4	
JBSG23-1	643	34.5797°N, 118.4597°W	sandstone	0.0054	39.4	0.0057	12.9	85.2	4	0.69	8.7	
-2				0.0068	42.8	0.0088	15.0	93.0	4	0.72	9.2	**8.9±0.2**
-3				0.0048	33.1	0.0111	42.2	151.8	5	0.63	8.9	
JBSG24-1	544	34.5820°N, 118.5578°W	sandstone	0.0062	43.3	0.0063	11.7	89.7	4	0.74	7.9	
-2				0.0081	45.7	0.0118	25.0	101.4	4	0.74	7.7	**7.9±0.1**
-3				0.0057	44.9	0.0126	30.8	174.3	4	0.73	8.0	

Sample	Elevation (m)	Latitude, Longitude	Rock type	Mass (mg)	mwar (μm)	He (pmol)	U (ppm)	Th (ppm)	# grains	F_T	Corr. age (Ma)	Avg. age (Ma)
LL1-1	1020	34.6738°N, 118.3944°W	monzonite	0.0120	49.0*	0.0011	10.4	33.6	4	0.72	15.3	**15.8±0.9**
-2				0.0180	59.0*	0.0012	10.2	31.6	4	0.76	16.0	
LL2-1	1005	34.5968°N, 118.3858°W	granite	0.0146	59.0*	0.0005	13.0	31.4	3	0.77	5.3	**5.4±0.3**
-2				0.0102	47.0*	0.0007	20.0	51.4	4	0.71	5.5	
LL4-1	1278	34.7293°N, 118.7098°W	granodiorite	0.0167	56.0*	0.0023	14.5	25.0	4	0.75	27.3	**27.5±1.7**
-2				0.0146	58.0*	0.0020	12.0	21.1	3	0.76	27.8	
LL5-1	1101	34.7287°N, 118.5912°W	granodiorite	0.0135	47.0*	0.0079	161.4	235.8	4	0.72	9.3	**10.6±0.6**
-2				0.0167	51.0*	0.0079	120.1	178.7	4	0.74	12.1	
LL6-1	1104	34.6805°N, 118.4436°W	granite	0.0148	51.0*	0.0016	20.2	41.7	4	0.74	13.5	**13.4±0.8**
-2				0.0229	55.0*	0.0019	23.2	49.3	5	0.75	13.2	
LL7-1	800	34.6447°N, 118.5107°W	diorite	0.0230	60.0*	0.0004	13.0	46.8	4	0.77	4.3	**4.6±0.3**
-2				0.0265	59.0*	0.0006	16.8	51.3	4	0.77	4.9	

Samples JBSG1-JBSG24 were analyzed at Virginia Tech; samples LL1-LL7 were analyzed at Caltech.
mwar = mass-weighted average radius; * indicates mean radius was used instead of mwar; Corr. = corrected.
‡ *14.5* and *2.6* Ma samples not used for average age calculation of JBSG9 and JBSG16, respectively.
Errors for Virginia Tech analyses are the average standard deviation of replicates, generally ~5% (1σ).
Errors for Caltech analyses are standard 6% (2σ) uncertainty expected for natural samples [*Farley* , 2002].
Latitude and longitude measured using North American Datum of 1927 Continental U.S. (NAD 27 CONUS).

Figures

Figure 2.1: Major structures of the Transverse Ranges in southern California plotted on a shaded relief map from a 30 m digital elevation model (NASA). Faults are based on data from the *California Division of Mines and Geology* [2000]. Boxed area is shown in Figure 2.2. Large arrow shows direction of Pacific plate motion relative to the North American plate [*DeMets et al*., 1990]. Hachured pattern shows area of San Gabriel and San Bernardino Mountains dated by (U-Th)/He and fission track techniques [*Spotila et al.*, 1998, 2001; *Blythe et al.*, 2000, 2002]. Abbreviations: LARSE—Los Angeles Regional Seismic Experiment, LSBM--Little San Bernardino Mountains, NSGM--northern San Gabriel Mountains, PR--Portal Ridge, SBM--San Bernardino Mountains, SEM--San Emigdio Mountains, SGM--San Gabriel Mountains, SJM--San Jacinto Mountains, YR--Yucaipa Ridge, *ECSZ*--eastern California shear zone, *EF*--Elsinore fault, *GF*--Garlock fault, *NFTS*--North Frontal thrust system, *PMF*--Pinto Mountain fault, *SAF*--San Andreas fault, *SGF*--San Gabriel fault, *SGPFZ*--San Gorgonio Pass fault zone, *SJF*--San Jacinto fault, *SMF*--Sierra Madre fault.

Figure 2.1: Major structures of the Transverse Ranges, southern California.

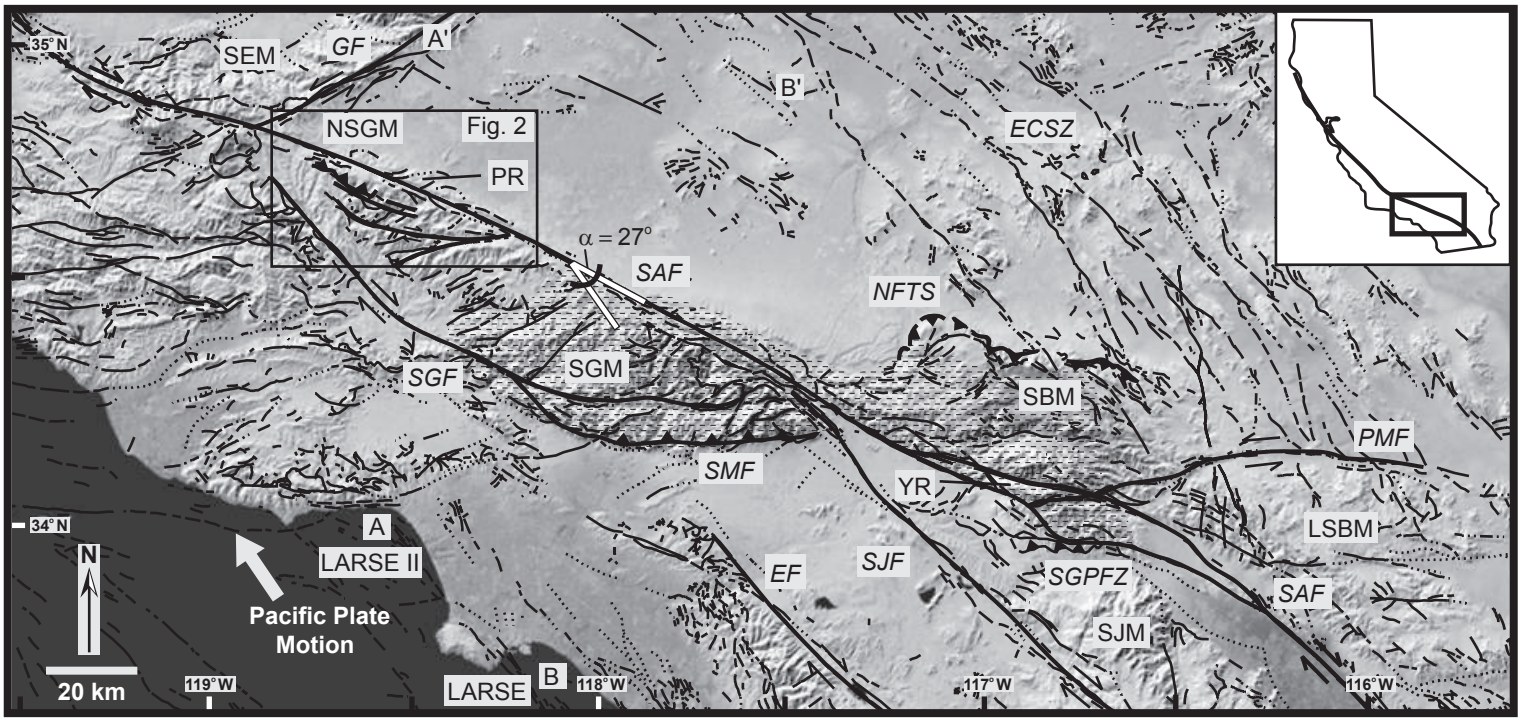

Figure 2.2: Geologic map of the NSGM based on data from *Jennings and Strand* [1969] and the *California Division of Mines and Geology* [2000] and plotted on a shaded relief map from a 30 m digital elevation model (USGS).

Figure 2.2: Geology of the NSGM.

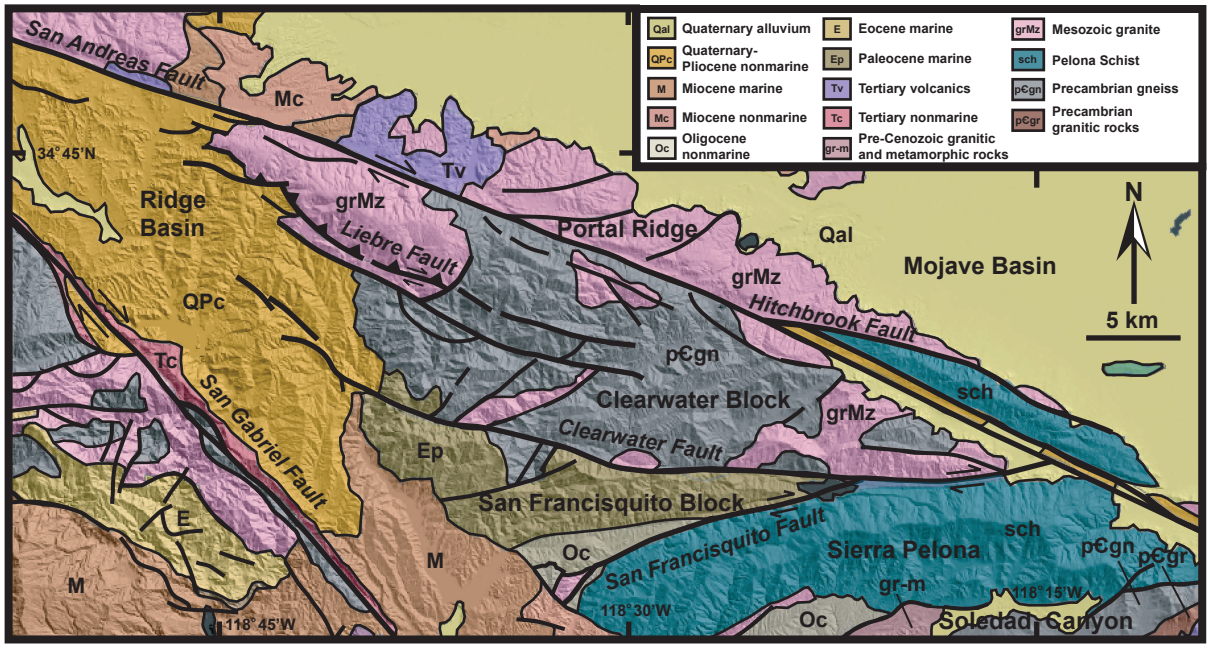

Figure 2.3: (a) Slope map of the NSGM. Slope determined by analyzing a 30 m digital elevation model from the USGS using ArcGIS, where slope is based on the elevation difference between a cell and the eight surrounding cells. Liebre and Sawmill Mountains and Portal Ridge are capped by low slopes interpreted to be erosional surfaces (circled), while Jupiter Mountain and adjacent peaks show few flat-topped areas. (b) Photographs of the NSGM landscape. Top: looking west-northwest at erosional surface found along Liebre Mountain (foreground) and Bald Mountain (middleground). Bottom: looking east-northeast at western flank of Jupiter Mountain. Photographs taken by Jamie T. Buscher. (c) Map of mean annual precipitation for the NSGM from 1900-1960 plotted on a shaded relief map from a 30 m digital elevation model (USGS). Precipitation values in inches for areas between rainfall contours. Data sources: USGS, California Department of Water Resources, and the California Division of Mines and Geology. Data acquired from the California Spatial Information Library (http://gis.ca.gov/). (d) Drainage map of the NSGM determined by analyzing a 30 m digital elevation model from the USGS using ArcGIS. Arrows denote general flow direction for major stream networks. Drainage basin abbreviations: RB--Ridge Basin, FC--Fish Canyon, ELC--Elizabeth Lake Canyon, SFC--San Francisquito Canyon, and LV--Leona Valley.

Figure 2.3: (a) Slope map; (b) Photos of area; (c) Precipitation map; (d) Drainage map.

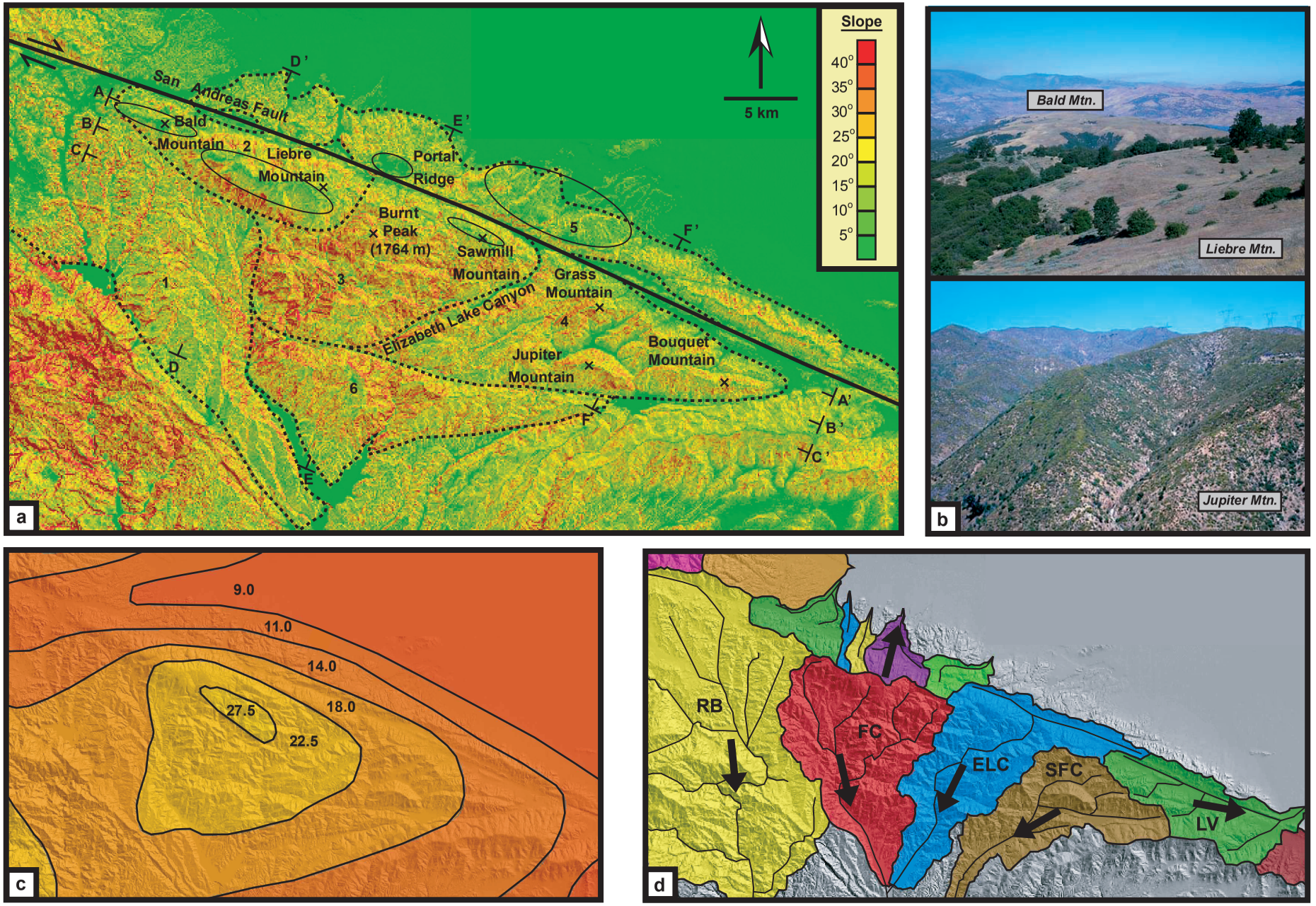

Figure 2.4: Along-strike (AA'-CC') and across-strike (DD'-FF') elevation profiles in the NSGM. Location of profiles shown in Figure 2.3a. Vertical exaggeration is 4:1. These profiles illustrate a scissoring of topography, from semi-planar, high-elevation ridges near the SAF that decay to the east (AA'; DD'-FF'), to the low elevation Ridge Basin that gives way to isolated, more rugged peaks on the east, farther away from the SAF (CC'; DD'-FF').

Figure 2.4: Along-strike and across-strike elevation profiles in the NSGM.

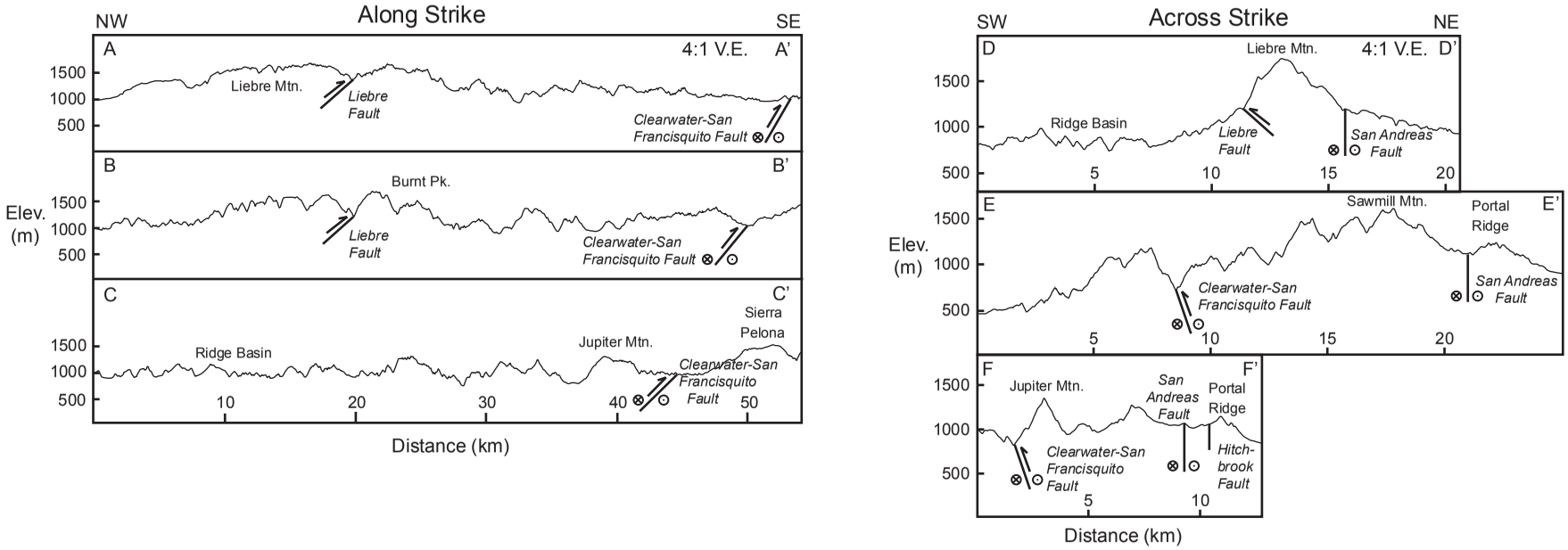

Figure 2.5: Distribution of AHe ages in the NSGM plotted on a shaded relief map from a 30 m digital elevation model (USGS). There is no concentration of young AHe ages near the SAF. The youngest ages in the NGSM are found in the southeastern portion of the Clearwater block, however these are approximately equidistant from the fault zone with the oldest ages implying differential cooling subparallel to the SAF.

Figure 2.5: Distribution of AHe ages in the NSGM.

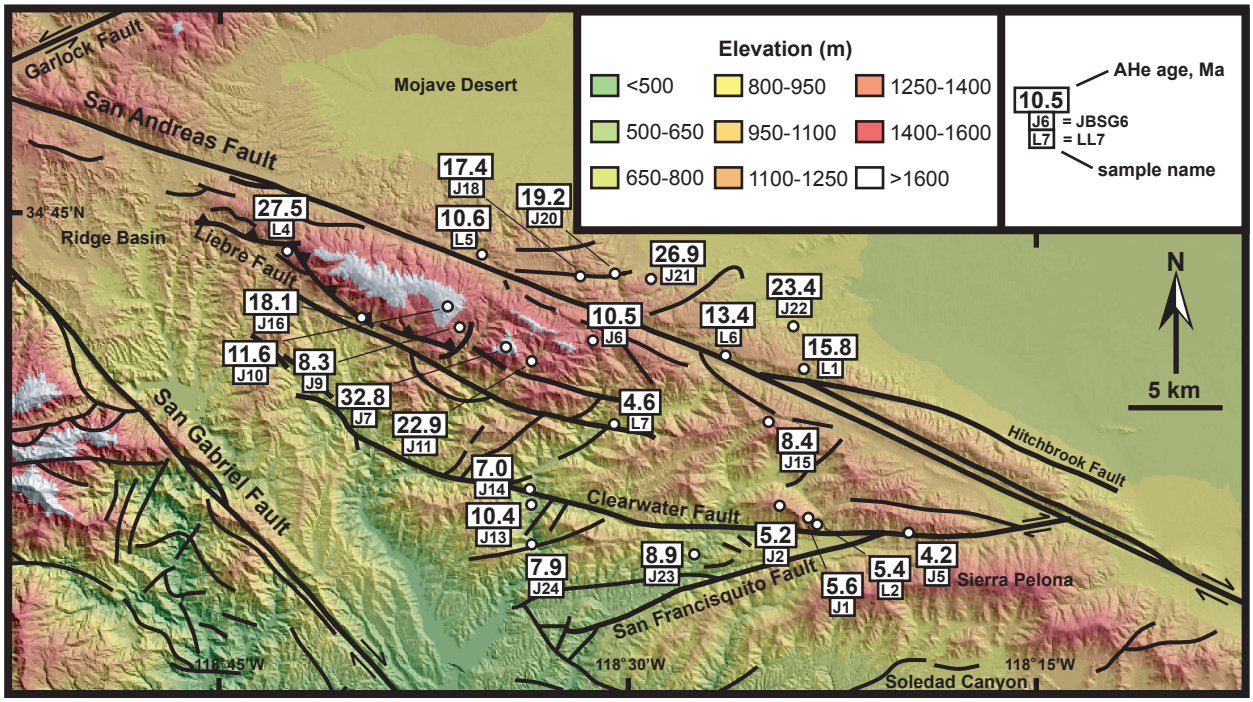

Figure 2.6: (a) AHe age plotted against distance perpendicular to the SAF in the NSGM. The lack of a distinct pattern suggests that fault proximity is not a primary influence on AHe age in the NSGM. (b) Distribution of sample elevations and ages projected to profile AA' in Figure 2.4 that extends along the Clearwater block subparallel to the SAF. Topographic profile is smoothed version of AA'. Portal Ridge samples are not plotted. Vertical exaggeration is 4:1. (c) AHe age plotted against elevation in the NSGM. Open circles denote samples from Jupiter Mountain and Burnt Peak. Open diamonds denote samples from Portal Ridge. Ages are nearly invariant with elevation at Jupiter Mountain, implying rapid denudation at 5 Ma, but two samples suggest a sharper change in age with elevation at Burnt Peak, implying much less exhumation. Error bars in both a and c are ±10% and ±6% of average age for Virginia Tech and Caltech samples, respectively.

Figure 2.6: (a) AHe age vs. Distance from SAF; (b) Elevation/AHe age vs. Distance along SAF; (c) Elevation vs. AHe age.

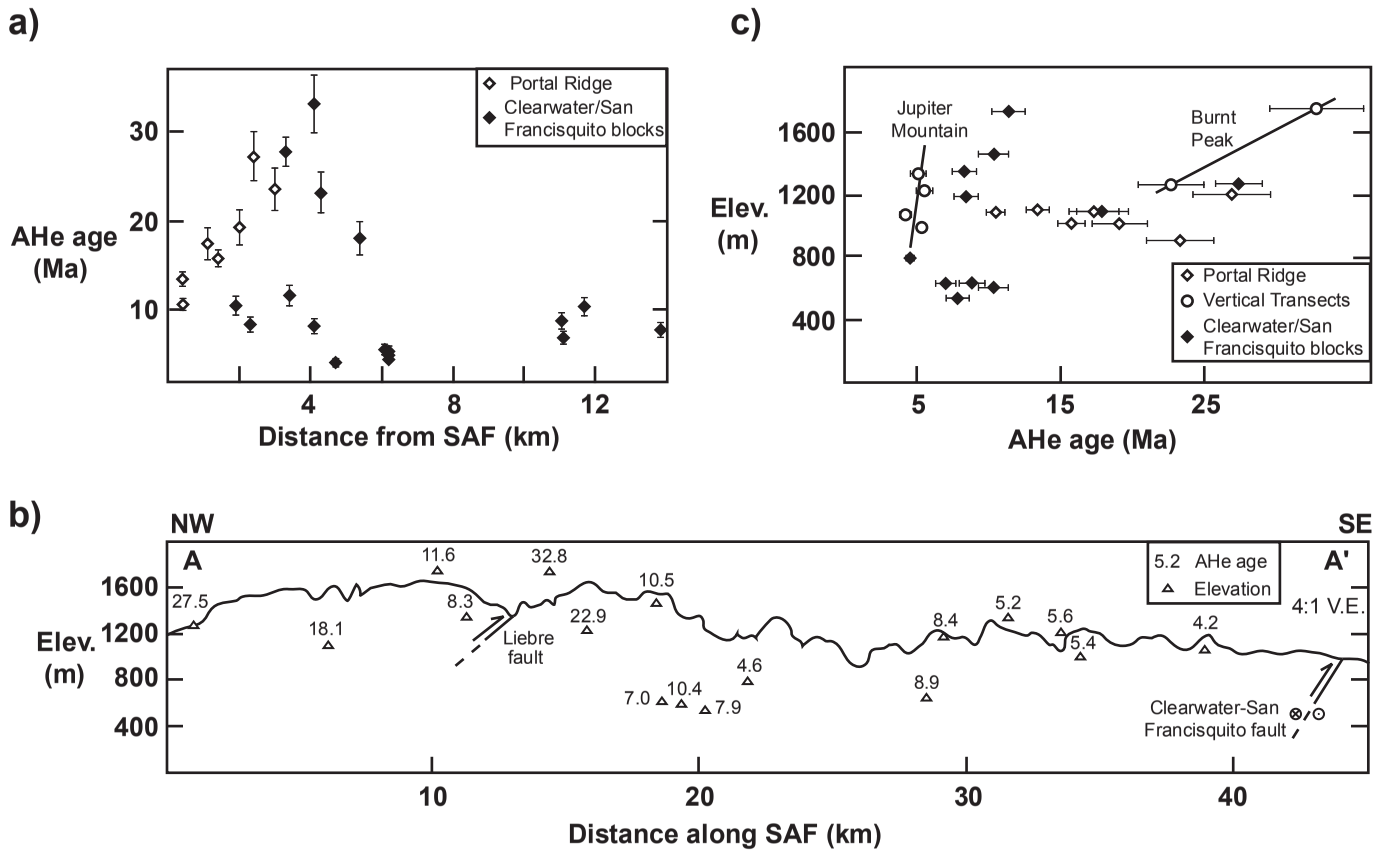

Figure 2.7: Tectonic development of the NSGM. (a) The San Gabriel fault was the primary Pacific-North America plate boundary fault at ~7 Ma, with some plate motion being accommodated by the Clearwater-San Francisquito and Squaw Peak-Liebre Mountain faults. (b) Primary plate motion was transferred from the San Gabriel fault to the SAF at ~5 Ma, possibly due to a change in Pacific plate motion. During this stepover across the Clearwater block, a restraining bend may have been created along the Squaw Peak-Liebre Mountain fault, causing the block to tilt top-up to the southeast as Pacific plate motion continued to the northwest. Small arrows show Pacific plate motion vectors before (open) and after (closed) ~5° clockwise rotation at ~5 Ma. (c) (Upper) One conceptual model (map view) of convergence during transition from the San Gabriel fault to the SAF. Sequential migration of activity from the Clearwater-San Francisquito fault (1), Squaw Peak-Liebre Mountain fault (2), and modern SAF (3) could trap blocks in local, northward-propagating restraining bends, such as shortening of the Clearwater block between stages (1) and (2). (Lower) Application of this model to specific fault orientations in the NSGM. Localized slip along these plate boundary faults, block rotations, and the geometry of the Squaw Peak-Liebre Mountain fault may have complicated tilting and exhumation of the NSGM. Black arrows show Pacific and North America plate motion directions post-5 Ma. (d) After this tilting event, the Clearwater block translated laterally along the SAF, with possibly little to no subsequent uplift in the last ~5 Ma. Abbreviations: CTM--

Circle-Table Mountain, CWB--Clearwater block, LM--Liebre Mountain, MB--Morongo block, RB--Ridge Basin, *BCF*--Blue Cut fault; *CWSF*--Clearwater-San Francisquito fault; *LF*--Liebre fault; *NSGF*--northern San Gabriel fault; *SLF*--Squaw Peak-Liebre Mountain fault. All other abbreviations are defined in Figure 2.1. Tectonic reconstructions in a, b, and d are syntheses of data from *Matti and Morton* [1993] and *Blythe et al*. [2002].

Figure 2.7: (a, b, and d) Location of mountain blocks and structures at ~7 Ma, ~5 Ma, and in the present day. (c) Conceptual model for fault propagation and subsequent block tilting (upper) and its application to the NSGM (lower).

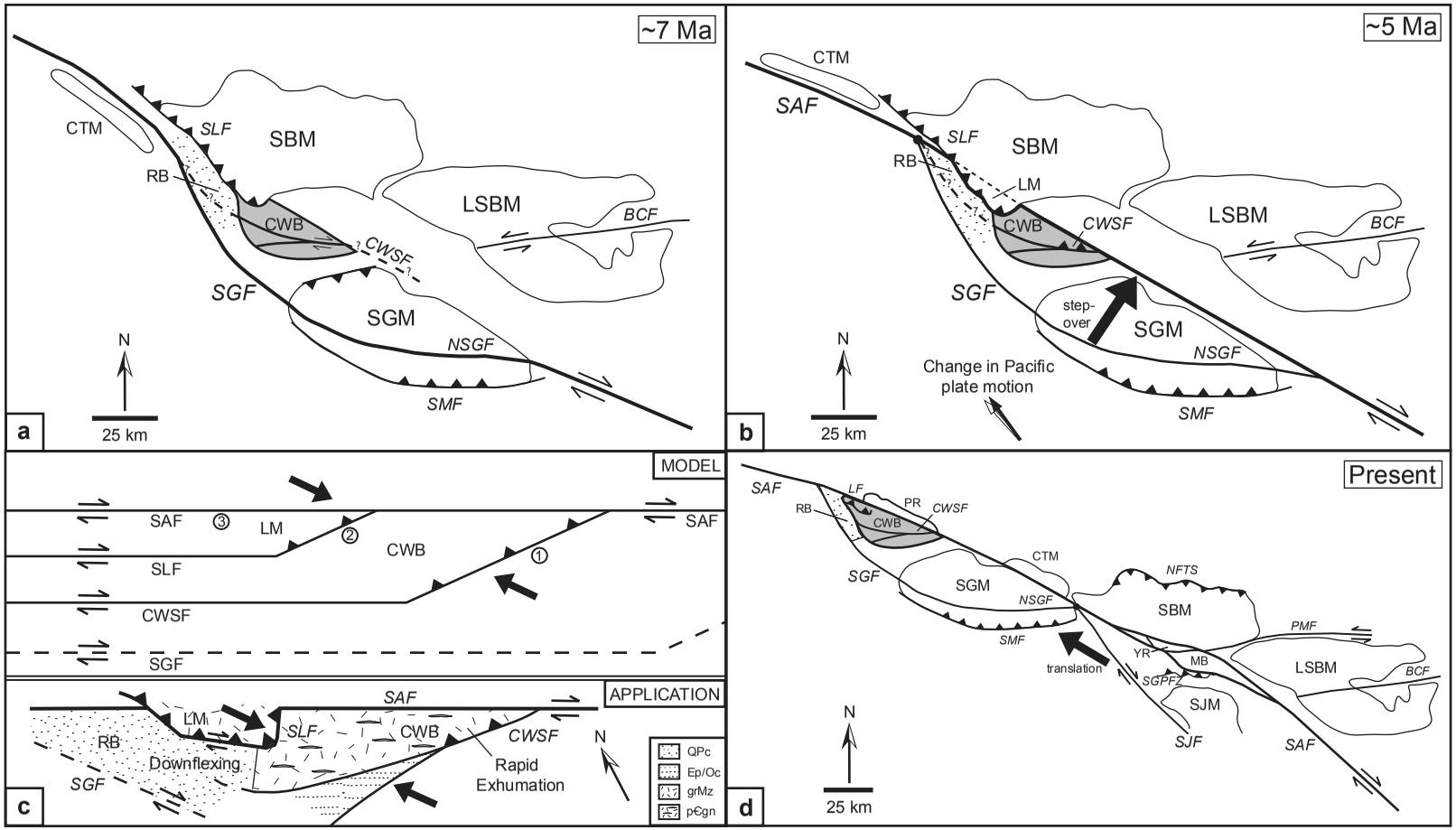

Figure 2.8: Conceptual model of heterogeneous near-field uplift in response to local structural complexities along a major strike-slip fault system. Because of the large rate of lateral motion, minor geometric complexities easily produce noticeable near-field convergence and uplift. Examples of such complexities are (1) local thrusting at a sharp restraining bend; (2) uplift of a crustal sliver along high angle faults at a gentle restraining bend; (3) local uplift due to slip transfer along a conjugate strike-slip fault; (4) local uplift due to slip transfer at the confluence of a subparallel strike-slip fault; (5) local uplift on a subsurface fault bend [e.g., *Meisling and Weldon*, 1989]. This model is well suited to the southern San Andreas fault, given the heterogeneous distribution of near-field uplift. Rather than accommodating oblique plate motion via wholesale shortening directly within the main fault zone, this model predicts convergence must be accommodated elsewhere, such as by distributed shortening in the far-field. PM--direction of plate motion, F_N--fault-normal velocity component, F_P--fault-parallel velocity component.

Figure 2.8: Conceptual model of heterogeneous near-field uplift in response to local structural complexities along a major strike-slip fault system.

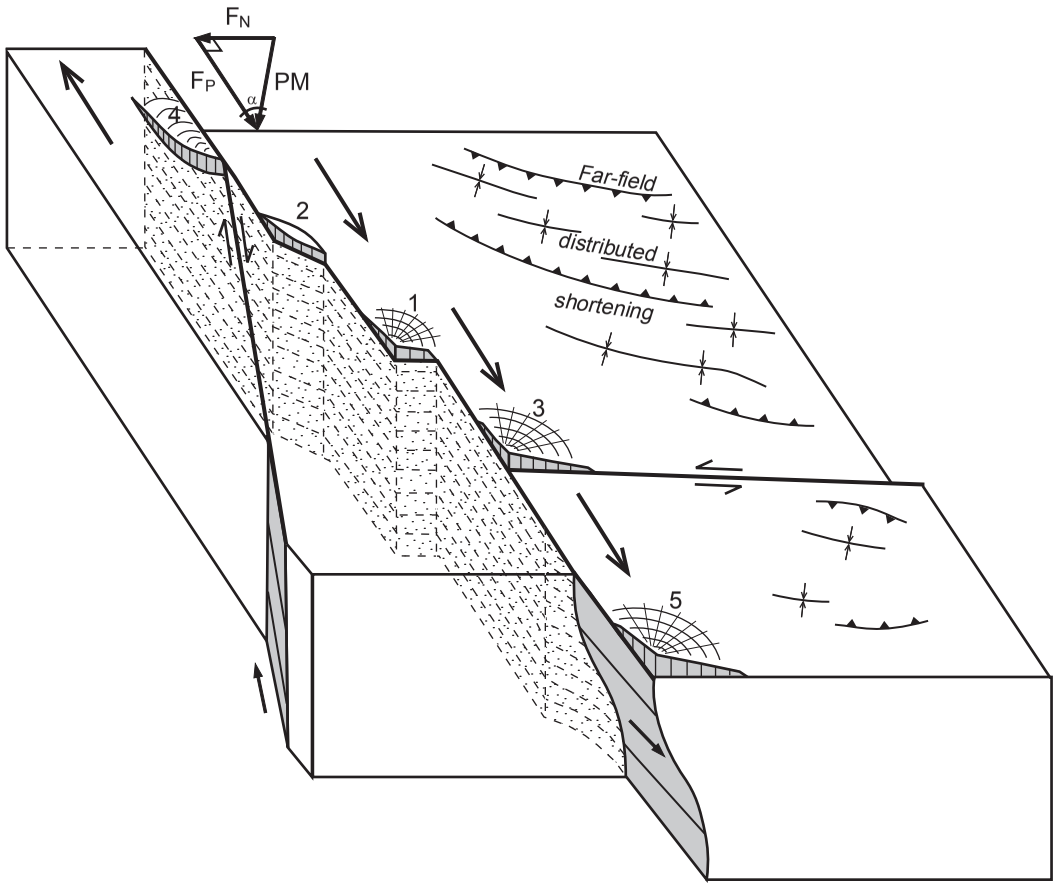

Chapter 3

Exhumation in the Chugach-Kenai Mountain belt above the Aleutian subduction zone, southern Alaska

JAMIE T. BUSCHER, AARON L. BERGER, and JAMES A. SPOTILA

Department of Geosciences, Virginia Polytechnic Institute and State University, Blacksburg, Virginia 24061, USA

Submitted to *American Geophysical Union, Chapman Monograph*, 2007

Abstract

Convergent deformation systems in continental backstops are a common component of well-coupled subduction zones worldwide. The Aleutian megathrust offshore southern Alaska has many attributes in common with convergent subduction zones observed elsewhere, implying significant permanent shortening could occur within the continental hanging wall. A continuous belt of rugged mountains occurs along the forearc of this subduction zone, from the Kenai Peninsula to the eastern Chugach Mountains near the Copper River, providing further evidence of active shortening. To test for long-term shortening and associated rock uplift along this forearc, we have analyzed bedrock samples from the Chugach and Kenai Mountains using low temperature thermochronometry. Fourteen new apatite (U-Th)/He ages from this area are older than expected based on the rugged topography, and imply minimal exhumation in the late Cenozoic in response to shortening within the forearc. Ages on the leeward side of this mountain belt are ~20-40 Ma and imply an average exhumation rate of ~0.1 mm/yr or less. Ages are younger along the coast (~12-18 Ma), implying slightly more rapid exhumation or deeper incision relative to mean elevation, perhaps due to greater precipitation along the windward flank of the range. Younger ages (~5 Ma) occur in the southeast near Cordova, and may result from local deformation associated with colliding and underthrusting of the Yaktuat microplate. However, all of these cooling ages are older than ages from

the Yakutat collision zone and along the transpressional Fairweather fault to the east, indicating that far less exhumation occurs in the backstop above the subduction zone. Based on these older ages and a mass balance interpretation of exhumation, we estimate that the long-term shortening in the forearc mountains above the Aleutian megathrust is less than 1 mm/yr.

Introduction

The Pacific-North America plate boundary in southern Alaska is marked by a continuous belt of mountainous topography, which extends seamlessly for more than 1000 km across zones of markedly different tectonic architecture (Figure 3.1). On the east, the Fairweather-Queen Charlotte transform boundary is lined by rugged coastal topography of the Coast and Fairweather Ranges. These mountains transition into the high St. Elias Range at the syntaxial bend in the plate boundary, where the Yakutat microplate is actively accreting to and subducting beneath the North American plate. High topography continues west of the Yakutat collision as the Chugach Mountains, which overlie the Aleutian megathrust and wrap around Prince William Sound to become the Kenai Mountains to the southwest. This contiguous arc of coastal mountains suggests that significant relative plate motion is being accommodated by crustal shortening within North America along the entire plate boundary, despite along-strike changes in the kinematics of deformation. Based on geologic and

thermochronologic investigations, the magnitude of shortening produced by transpression along the transform margin and collision along the Yakutat margin is approximately known [*Spotila et al.*, 2004; *Bruhn et al.*, 2004; *McAleer and Spotila*, in prep., *Berger et al.*, in prep.; *Meigs et al.*, in prep.]. However, the magnitude of long-term continental convergence accommodated above the Aleutian subduction zone has not yet been quantified.

The Chugach and Kenai Mountains may represent active crustal shortening in the hanging wall of the Aleutian megathrust, similar to the mountain building that occurs in other forearcs of convergent, highly-coupled, low-angle subduction zones. Permanent shortening in overriding continental plates may be produced by compression associated with high frictional resistance along the plate interface [*Gutscher et al.*, 2000], such as that associated with the Nankai trench of Japan [*Hasegawa et al.*, 2000; *El-Fiky and Kato*, 2006] or flat-slab subduction of the Andean subduction zone and the corresponding fold and thrust belt of the Andean arc [*Gutscher et al.*, 2002; *Trenkamp et al.*, 2002; *McQuarrie et al.*, 2005]. In the Aleutian subduction zone, the Pacific plate consists of relatively young oceanic crust and subducts at a low angle [*Fuis and Plafker*, 1991; *Ratchkovsky and Hansen*, 2002], suggesting the plate interface should be well coupled. Given that great earthquakes usually occur along convergent, well-coupled subduction zones, the occurrence of the M9.2 megathrust event on the Aleutian subduction zone in 1964 [*Doser et al.*, 1999] is indicative of a

subduction zone in which upper plate deformation might be expected. Upper plate deformation can be enhanced by subduction of buoyant features or asperities in a subducting slab, such as with the subduction of an extinct oceanic ridge like that along the Middle America Trench where the Cocos Ridge is generating convergence and uplift of the overlying Costa Rican arc [*Gräfe et al.*, 2002; *Fisher et al.*, 1998]. Seafloor roughness of the subducting plate also exists in the Aleutian trench [*Fruehn et al.*, 1999]. Convergence and rock uplift in a forearc setting may also result from underplating and accretion of sedimentary or oceanic material, such as with the subaerial orogenic wedges built from subduction complexes in the Olympic Mountains of the northwestern United States [*Brandon et al.*, 1998; *Batt et al.*, 2001] and the Caribbean arc [*Westbrook et al.*, 1988]. Terrane accretion and underplating have been active throughout the Mesozoic and Cenozoic at the Aleutian trench [*Plafker et al.*, 1994].

Although the rugged topography of the Chugach-Kenai Mountains qualitatively implies substantial active upper plate shortening (Figure 3.2), topography alone does not quantify the magnitude of convergence accommodated by the Alaskan forearc. An estimate of shortening based on the crustal thickening required to produce the mean elevation of the ranges cannot be made, because the original crustal thickness is not known and the three-dimensional crustal geometry of the forearc is controlled by the gently-dipping subducting slab at ~20-35 km depth (Figure 3.3) [*Fuis and Plafker*, 1991]. Furthermore, subduction zones may

produce dynamic topography as a result of mantle buoyancy [*Hager*, 1984; *Husson*, 2006], such that forearc topography may not be purely isostatic and by itself is not an accurate measure of the permanent shortening that has occurred. To obtain a measure of the long-term (10^6 yr), permanent shortening accommodated by the Chugach-Kenai Mountains, we have used low-temperature thermochronometry to estimate the magnitude and rate of recent exhumation associated with upper plate convergence. Fourteen new apatite (U-Th)/He ages (AHe), coupled with previously measured AHe and apatite fission-track ages (AFT) to the east, show that, although topography is nearly as rugged as that in the Yakutat collision zone, minimal Neogene exhumation has occurred in the forearc above the Aleutian subduction zone.

Tectonics of the Chugach-Kenai Mountains

The hanging wall of the Aleutian subduction zone consists of rocks that were accreted to the North America plate during earlier phases of Kula and Pacific plate subduction [*Plafker et al.*, 1994]. The Chugach and Kenai Mountains consist predominantly of metaturbidites (phyllite, graywacke, argillite) and local Eocene intrusions of the Chugach terrane, which formed as an accretionary prism complex and was subsequently metamorphosed in the Cretaceous to early Teritary [*Plafker et al.*, 1994; *Little and Naeser*, 1989]. This terrane is bound on the south by the structurally lower and younger Prince William terrane that consists of

deformed Paleocene to lower Eocene trench-fill turbidite sequences. The high topography of the Chugach and Kenai Mountains terminates northwards at about the position of the Border Ranges fault, along which the Chugach terrane was underthrust beneath older crystalline basement rocks of the Peninsular terrane in the late Mesozoic [*Little and Naeser*, 1989; *Plafker et al.*, 1994]. Beneath these terranes, north-dipping slabs of oceanic crust and related accretionary assemblages have been underplated to the North American plate and now lie above the active megathrust [*Fuis and Plafker*, 1991].

Since most structures within the Chugach and Kenai Mountains were active during terrane accretion and thus predate the modern plate boundary architecture, a geological synthesis of active shortening normal to the plate boundary through this belt has not been made. Active deformation does occur northwest of these ranges in the Cook Inlet basin, a forearc basin filled with Late Cretaceous through Quaternary sediments. Neogene thrusting and fault-related folding in this basin have resulted from a combination of thrust-type simple shear due to resistance on the underlying megathrust and dextral transpression associated with counterclockwise rotation and extrusion of the Southern Alaska block along the dextral Denali and Castle Mountain faults [*Haeussler et al.*, 2000; *Flores and Doser*, 2005; *Bruhn and Haeussler*, 2006]. This oblique compression is partly driven by convergence of Yakutat collision to the east, which is thought to affect the deformation pattern of nearly all of Alaska [*Lahr and Plafker*, 1980;

Pavlis et al., 2004; *Bruhn and Haeussler*, 2006]. Another belt of active reverse faulting occurs southeast of the Kenai Peninsula. A splay thrust within the North American backstop of the megathrust known as the Patton Bay fault produced as much as 11 m of uplift on Montague Island during the 1964 earthquake [*Malloy*, 1964], implying coseismic shortening in the upper plate of the subduction zone. Like the Cook Inlet structures, however, the total long-term shortening accommodated by this thrust is likely minor. It is unclear how the topography of the Chugach and Kenai Mountains relates to active deformation that occurs in these zones.

Active deformation of the Aleutian forearc is also apparent in post-seismic surface deformations based on GPS observations since 1964. The Kenai Peninsula experienced primarily coseismic subsidence, but has since experienced as much as several meters of surface uplift [*Cohen and Freymueller*, 2004]. Recent horizontal displacements in the peninsula are variable. In the northeast, displacement vectors are towards the northwest, consistent with accumulation of convergent strain due to locking of the megathrust [*Freymueller et al.*, 2000; *Zweck et al.*, 2002]. In the southwestern Kenai Peninsula, surface displacements are directed to the southeast, due to continued post-seismic afterslip below the 1964 rupture area [*Zweck et al.*, 2002]. This displacement pattern also suggests that the megathrust interface is heterogeneously coupled, with greater coupling and frictional resistance in the northeastern Kenai Peninsula and Prince William

Sound than in the western Kenai and Cook Inlet [*Zweck et al.*, 2002]. A variable pattern of coupling could affect the distribution of shortening and uplift in the overlying plate. Given a continued post-seismic response, the complexities of asperities along the megathrust interface, and the impact of isostatic adjustment to deglaciation [*Larson et al.*, 2005], it is unclear what the decadal displacement field means for the long-term uplift of the Chugach and Kenai Mountains.

Topography of the Chugach-Kenai Mountains

The topography of the Chugach and Kenai Mountains are comparable in ruggedness to the landscape within the core of the St. Elias Mountains in the Yakutat collision zone. High, steep topography extends continuously across the Copper River and the transition from active microplate collision in the east to subduction in the west (Figures 3.1 and 3.2). To quantify variations in elevation and slope between these two regions, 60 m digital elevation models (USGS) were analyzed using ArcGIS. Mean elevation of the mountainous area between the Copper River and Yakutat Bay is slightly higher (1356 m) than in the Chugach (1091 m) and Kenai (688 m) Mountains to the west of the Copper River. Maximum elevation of these regions is more distinct, decreasing from 5968 m in the Yakutat collision zone to 3979 m in the Chugach Mountains north of Prince William Sound and 1992 m in the Kenai Peninsula. Mean slope shows the opposite trend; it is slightly higher in the Chugach and Kenai Mountains (19^{o} and

17°, respectively) than in the collision zone itself (16°, excluding the coastal extent of large piedmont glaciers) (Figure 3.4). The landscape is actually more rugged than implied by these mean slopes, given that low-gradient glacier surfaces and deglaciated, incised glacial valleys snake throughout these ranges and dampen the means. The bedrock ridges and peaks between glaciers are much steeper than these mean values. The lower mean slope of the active Yakutat collision zone is also likely a result of its greater fraction of glacier surface area than in the Chugach and Kenai Mountains. These ranges are thus roughly comparable in ruggedness, despite the changes in tectonics east and west of the Copper River. The widespread ruggedness may result from vigorous late Cenozoic glacial erosion along the entire coastal mountain belt [*Péwé*, 1975].

Within the Chugach and Kenai Mountains, several topographic features deserve special notice. The highest area occurs just north of Prince William Sound, where the topography forms a steep south-facing massif at the northern apex of the mountain belt as shown in an across-strike topographic profile (Figure 3.5a). This area corresponds to a region of particularly high slope (Figure 3.4), and may be a locus of rock uplift. Elevation decreases irregularly along-strike from this topographic apex for ~50 km to the east and west (Figure 3.5b). Beyond this zone in both directions, peak elevations are roughly concordant at ~1-1.5 km, and can be joined by semi-planar envelopes of the maximum topography that extend for 100-150 km across the strike of the range and are interrupted by glacial

valleys that are incised to near sea level (Figures 3.5c and d). Although peaks can be connected by these imaginary surfaces, the topography still appears very rugged. The entire coastal mountain belt consists of sharp peaks and ridges, arêtes, and steep valley walls and fjords, as is typical of a landscape affected by vigorous glacial erosion. This ruggedness gives the region a youthful topographic expression, which suggests recent, rapid mountain building. However, given the lack of data on surface uplift or exhumation history, we can not yet draw inferences on what these mountains mean as far as recent tectonic deformation.

Thermochronometric Approach

To investigate the occurrence of permanent shortening and rock uplift in the hanging wall of the Aleutian subduction zone, we have used low-temperature thermochronometry to estimate Neogene exhumation in the Chugach and Kenai Mountains. Fourteen new (U-Th)/He ages (AHe) were obtained on bedrock samples collected primarily along roads but also locally by helicopter (Figure 3.6). This sample set is reconnaissance in nature, and future work is required to fill in gaps and provide vertical sampling transects. Our research strategy included sample collection from several trench-normal transects spanning the windward and leeward sides of the mountain belt. These samples provide new thermochronometric coverage of southern Alaska between Seward and the Copper River and expand on isolated apatite fission track ages (AFT) measured

by *Little and Naeser* [1989] and *Plafker et al.* [1989]. Considerably more low-temperature cooling data exists for the region east of the Copper River, in the Yakutat collision zone [*Spotila et al.*, 2004; *Berger et al.*, in prep.]. These data make for an interesting comparison between cooling histories in the collision zone versus the upper plate of the subduction zone.

Apatite (U-Th)/He dating is a low-temperature thermochronometer with a closure temperature range of ~50-90°C, depending primarily on grain size and cooling history [*Wolf et al.*, 1996; *Farley*, 2000; *Ehlers and Farley*, 2003]. AHe ages can be interpreted to represent the time since bedrock samples exhumed through depths corresponding to closure temperatures, or from ~2-3 km depth for the regional geothermal gradient of ~25°C/km in the Chugach-Kenai Mountains [*Magoon*, 1986; *Johnsson et al.*, 1992; *Johnsson and Howell*, 1996]. Interpretation of exhumation using apparent AHe cooling ages is actually more complex, as cooling may be affected by advection of isotherms associated with rapid denudation or variable isotherm shape due to overlying topography [*Ehlers and Farley*, 2003; *Reiners and Brandon*, 2006]. For reasonably slow exhumation rates (<1 mm/yr) and a moderate geothermal gradient, however, the closure temperature approach places a reasonable constraint on the long-term average exhumation history of a bedrock sample.

AHe ages were measured at Virginia Tech. Aliquots ranging from 1-24 apatite grains were degassed at 940°C in a resistance furnace for 20 minutes and

analyzed for ^{4}He contents using a ^{3}He spike and quadrupole mass spectrometry. U and Th contents were measured on the same samples by isotope dilution using ICP mass spectrometry at Caltech. Uncertainties associated with each analytical measurement, including the estimation of the alpha ejection factor based on grain size and shape, combine to yield expected errors in ages of ±10% (2σ). Reproducibility of natural samples is typically comparable to this, such as the repeatability of the standard Durango fluorapatite age at Virginia Tech of 30.9±1.53 Ma (1σ; n=40), relative to the known cooling age of 31.44 Ma [*McDowell et al.*, 2005]. The accuracy of measured ages is increased by measuring multiple (2-6) aliquots from the same sample and using the average result (Table 3.1). In some cases, anomalously old outlier ages emerge, presumably due to the presence of U- and Th-bearing microinclusions that were missed during sample screening and selection. These outliers are generally removed from the average results prior to interpretation (Table 3.1).

Results and Interpretations

Measured AHe ages from the Chugach and Kenai Mountains are older than expected, based on the rugged topography and the likelihood for active shortening in the upper plate of the well-coupled Aleutian megathrust. The oldest ages occur on the leeward side of the mountain belt, where AHe ages are ~20-40 Ma (Figure 3.6; Table 3.1). These ages are similar to the ~28-32 Ma AHe ages

measured at the northwestern margin of the Yakutat collision east of the Copper River, which were considered to reflect "background" exhumation rates outside of the collision zone by *Spotila et al.* [2004]. They are also consistent with the AFT ages in the region of 17-42 Ma [*Little and Naeser*, 1989; *Plafker et al.*, 1989]. These data imply that the long-term average exhumation rates from the northern Chugach-Kenai mountain belt have been <0.1 mm/yr.

AHe ages are slightly younger towards the core of the mountain belt and closer to the coast. AHe ages are 12-18 Ma in the center of the range. Several younger ages (~5 Ma) occur in the far southeast, near Cordova (Figure 3.6). Ages are thus correlated with distance from the coast in both the Kenai and Valdez areas (Figure 3.7a). This trend implies greater denudation along the southern, windward flank of the mountains, which can be interpreted in two ways. First, ages may be treated statically and used to calculate the long-term average exhumation rate using a closure-temperature approach. In this case, ages along the coast, excluding the youngest samples near Cordova, imply exhumation rates of ~0.2 mm/yr, or about double that estimated for the northern flank of the range. Alternatively, these ages may reflect non-horizontal isochrons and variation in structural sampling depth relative to the mean elevation of the concordant summit surfaces. If AHe isochrons parallel the envelopes of maximum topography illustrated in Figures 3.5c and 3.5d, the southern samples are structurally lower than the northern samples, such that they should be younger if ages decrease with

structural depth. This is consistent with the overall correlation between age and elevation in the Valdez area (Figure 3.7b), where the summit surface is close to horizontal. The lack of an age-elevation correlation in the Kenai area is also consistent, given that the summit surface is not horizontal but is tilted towards the north (Figure 3.5c). This interpretation still implies greater erosion on the south, however, as more incision below the summit surface is required to produce the greater relief between summits and the valleys where samples were taken. Whether interpreted in terms of average rates or incision into isochrons, the younger ages thus imply greater denudation along the coast.

No samples were obtained from the core of the Chugach Mountains north of Prince William Sound, which is the highest and steepest part of the mountain belt (Figure 3.5a). Whether cooling ages are younger in this region due to greater incision and rock uplift, remains to be tested by future work. Given that our samples are all generally from single elevations, future work will also be required to test whether age-elevation relationships within this area provide constraints on the history of exhumation in the Oligocene and Miocene.

The younger AHe ages (~5 Ma) that occur along the coast in the easternmost part of the study area by the Copper River may also be interpreted as resulting from more rapid long-term average exhumation rates (Figure 3.6). These ages imply exhumation rates approaching 0.5 mm/yr, based on closure-temperature interpretation. The most likely cause of this greater exhumation is

proximity to the trench and the deformation front of the Yakutat collision zone (Figure 3.1). These young samples are roughly the same distance from the trench as Montague Island, where active reverse faulting occurred in the hanging wall of the subduction zone during the 1964 earthquake [*Malloy*, 1964]. The greater exhumation recorded by these samples could thus reflect splay thrusting on yet-to-be-discovered faults in an arc that wraps around the trench from Montague Island through Cordova to the Bagley Icefield on the east, where similar deformation has been argued for along the Contact fault at the same distance from the trench [*Berger et al.*, in prep.]. Alternatively, the deformation responsible for these young ages may result from proximity (~100 km) to intense shortening in the Pamplona Zone near Kayak Island, an offshore fold and thrust belt that curves around from the core of the Yakutat collision zone to connect with the Aleutian megathrust [*Plafker et al.*, 1994; *Bruhn et al.*, 2004]. A final contributor to the exhumation recorded by these samples is surface processes. *Spotila et al.* [2004] observed an increase in long-term exhumation rate towards the coast in the core of the Yakutat collision zone, and speculated that this was due to a southward increase in orographic precipitation and resulting drop in glacier equilibrium line altitude [*Péwé,* 1975]. *Berger et al.* [in prep.] identify, with more certainty, a focusing of denudation by glacial erosion. A similar effect could be at work in the Chugach-Kenai mountain belt, although additional sampling would be required to test this hypothesis.

In contrast to the limited exhumation implied by our new ages from the Chugach and Kenai Mountains, AHe ages are much younger (as young as 0.4 Ma) and imply far more rapid exhumation (~5 mm/yr maximum) in the core of the Yakutat collision zone and St. Elias Mountains to the east [*Spotila et al.*, 2004; *Berger and Spotila*, 2006; *Berger et al.*, in prep]. Although the mountains east and west of the Copper River appear comparably rugged on both shaded-relief and slope maps (Figures 3.1 and 3.4), the long-term denudation of these tectonically-distinct regions is thus different. It is no surprise that exhumation rates are so rapid in the St. Elias range, where collision of the Yakutat microplate results in 2-3 cm/yr shortening within the coastal fold and thrust belt [*Plafker et al.*, 1994; *Bruhn et al.*, 2004; *Spotila et al.*, 2004; *Berger et al.*, in prep.]. The minimal exhumation from the Chugach-Kenai Mountains, however, implies relatively little (if any) long-term active shortening in the upper plate of the Aleutian megathrust. This is somewhat of a surprise given the apparent ruggedness of these mountains, which implies relatively recent and vigorous mountain building.

Discussion and Conclusions

Regional exhumation rates in the majority of the Chugach and Kenai Mountains averaged over the past few tens of millions of years of subduction history can not have exceeded ~0.2 mm/yr based on AHe data obtained so far. This significantly limits the amount of permanent shortening that may have been

occurring in the forearc ridge above the megathrust. If the forearc has maintained an approximately constant geometry since accretion of the Prince William terrane in the mid-Cenozoic, crustal mass balance implies that less than 1 mm/yr of shortening would be required to produce such slow exhumation across the entire ~100-km-wide, ~20-35-km-thick belt of mountainous crust in the upper plate of the subduction zone. The total magnitude of rock uplift that could have occurred since cooling of samples below closure temperatures in the Miocene is only ~2.5 km, including ~1 km of surface uplift based on the mean elevation of these ranges and ~1.5 km of exhumation from above the concordant summit surfaces. This minor exhumation could have gone undetected by the cooling of bedrock samples from the valleys sitting ~1 km below the summit surfaces. This minor rock uplift could have proceeded at a slow, steady rate since the mid-Tertiary, or could have been punctuated. Unfortunately, the AHe ages do not better constrain the history of exhumation, and it is unclear when surface uplift in this region initiated. Paleogeographic evidence suggests uplift of mountains in southeastern Alaska starting in the late Miocene, but the exact timing of uplift of the Kenai or western Chugach Mountains is not known [*White et al.*, 1997]. Nonetheless, the lack of rapid exhumation from these ranges implies that little permanent shortening has occurred in the North America plate in response to Pacific plate subduction.

Although some rock uplift and mountain building have certainly occurred in the Chugach and Kenai Mountains in the late Cenozoic, the minimal amount of

shortening that could have been accommodated goes against expectations for such a convergent subduction zone. The Aleutian megathrust is well-coupled, as implied by the occurrence of great earthquakes and the modern accumulation of elastic strain [*Doser et al.*, 1999; *Cohen and Freymueller*, 2004]. The downgoing oceanic slab is also relatively young, shallowly-dipping [*Fuis and Plafker*, 1991; *Fruehn et al.*, 1999; *Ratchkovsky and Hansen*, 2002; *Veilleux and Doser*, 2007], rough [*Fruehn et al.*, 1999], and the margin has experienced significant accretion and underplating [*Fuis and Plafker*, 1991; *Plafker et al.*, 1994], all pointing to a likelihood of active shortening in the forearc. In contrast, other convergent subduction zones show greater evidence for active forearc shortening in the form of younger AHe and AFT cooling ages. Examples include cooling ages as young as 2 Ma in the Olympic Mountains [*Brandon et al.*, 1998; *Batt et al.*, 2001], 5 Ma in the Andes [*Benjamin et al.*, 1987; *Coughlin et al.*, 1998], 1.7 Ma in the Costa Rican forearc [*Gräfe et al.*, 2002], 3 Ma in the Kamchatka peninsula [*Freitag et al.*, 2001], and 6 Ma in the Kyushu and Kii regions of southwestern Japan [*Hasebe and Tagami*, 2001].

Although our data argue that the total permanent shortening of the North American forearc must have been limited in the late Cenozoic, the data do not by themselves indicate what the cause of this minor rock uplift of the Chugach and Kenai Mountains has been. It is possible that this uplift has resulted from minor shortening of the upper plate above the subduction zone. It is also possible,

however, that this uplift has resulted from dynamic forces associated with mantle density contrasts or flexure of the hanging wall lithosphere [*Hager*, 1984; *Husson*, 2006]. The spatial relationship of this arcuate mountain belt and the location of the trench and the zones of coseismic vertical displacements in 1964 argue that uplift has been related to subduction zone processes in some way. In another convergent subduction zone, the Cascadia margin of western North America, relationships have been observed between along-strike variations in mean topography and the characteristics of subduction (i.e. velocity, age, and buoyancy of the downgoing slab) [*Kelsey et al.*, 1994]. However, the relationships between upper plate topography and frictional coupling along a megathrust are complex [*Song and Simons*, 2003; *Fuller et al.*, 2006]. Other variables such as along-strike strain accumulation or variations in subduction zone attributes can also complicate the nature of deformation in the overriding plate [*Prawirodirdjo et al.*, 1997; *Miller et al.*, 2001; *Mazzotti et al.*, 2002]. Additional investigations are required before we can understand how the Chugach-Kenai Mountain belt relates to strain along the Aleutian subduction zone.

Finally, the lack of rapid Neogene exhumation in these ranges is surprising for a humid, temperate glaciated mountain belt. In other mountain belts that have experienced wet-based glacial erosion in the late Cenozoic, evidence suggests that onset of glaciation strongly enhanced regional exhumation rates. For example, AHe ages in British Columbia's Coast Ranges as young as 1.5 Ma have been

interpreted to result purely from recent exhumation due to rapid glacial erosion, in the absence of tectonic drivers [*Farley et al.*, 2001; *Shuster et al.*, 2005; *Ehlers et al.*, 2006; *Densmore et al.*, 2007]. Late Cenozoic increases in erosion and sedimentation due to glaciers have been inferred in other temperate glaciated mountain belts as well [*Reiners et al.*, 2003; *Hebbeln et al.*, 2007; *Haeuselmann et al.*, 2007]. Given that the Chugach and Kenai Mountains receive precipitation of >2 m/yr along the coast, and that glacier equilibrium line altitudes were as low as 0.3 km during the last glacial maximum [*Péwé*, 1975], it would seem that rapid glacial erosion would be as likely to occur here as anywhere else. This is particularly true, given that this is also an active tectonic margin, at which there may be a tectonic driver of rapid rock uplift as well. The lack of sustained rapid glacial erosion during the late Cenozoic in the Chugach-Kenai Mountains brings to question the validity of whether glacial erosion, by itself, has been responsible for increases in erosion observed with thermochronometry in other temperate coastal mountain belts.

Acknowledgements

We thank the conveners of the 2006 Chapman Conference on Alaska tectonics for creating the stimulating intellectual environment in which the idea for this paper was hatched. Lindsey Hedges at Caltech is thanked for assistance with ICP-MS analyses.

References

Batt, G.E., M.T. Brandon, K.A. Farley, and M. Roden-Tice (2001), Tectonic synthesis of the Olympic Mountains segment of the Cascadia wedge, using two-dimensional thermal and kinematic modeling of thermochronological ages, *J. Geophys. Res.*, *106*, 26,731-26,746.

Benjamin, M.T., N.M. Johnson, and C.W. Naeser (1987), Recent rapid uplift in the Bolivian Andes: Evidence from fission-track dating, *Geology*, *15*, 680-683.

Berger, A.L. and J.A. Spotila (2006), Strain partitioning within the western Chugach-St. Elias orogen, Alaska: The effect of glacial erosion, *Geol. Soc. Am. Abstr. Programs*, *38*, 450.

Brandon, M.T., M.K. Roden-Tice, and J.I. Garver (1998), Late Cenozoic exhumation of the Cascadia accretionary wedge in the Olympic Mountains, northwest Washington State, *Geol. Soc. Am. Bull.*, *110*, 985-1009.

Bruhn, R.L. and P.J. Haeussler (2006), Deformation driven by subduction and microplate collision; Geodyanmics of Cook Inlet Basin, Alaska, *Geol. Soc. Am. Bull.*, *118*, 289-303.

Bruhn, R.L., T.L. Pavlis, G. Plafker, and L. Serpa (2004), Deformation during terrane accretion in the Saint Elias orogen, Alaska, *Geol. Soc. Am. Bull.*, *116*, 771-787.

Cohen, S.C. and J.T. Freymueller (2004), Crustal deformation in southcentral Alaska: The 1964 Prince William Sound earthquake subduction zone, *Adv. Geophys.*, *47*, 1-63.

Coughlin, T.J., P.B. O'Sullivan, B.P. Kohn, and R.J. Holcombe (1998), Apatite fission-track thermochronology of the Sierras Pampeanas, central western Argentina: Implications for the mechanism of plateau uplift in the Andes, *Geology*, *26*, 999-1002.

DeMets, C., R.G. Gordon, D.F. Argus, and S. Stein (1990), Current plate motions, *Geophys. J. Int.*, *101*, 425-478

Densmore, M.S., T.A. Ehlers, and G.J. Woodsworth (2007), Effect of Alpine glaciation on thermochronometer age-elevation profiles, *Geophys. Res. Lett.*, *34*, L02502, 6 p.

Doser, D.I., A.M. Veilleux, and M. Velasquez (1999), Seismicity of the Prince William Sound region for over thirty years following the 1964 Great Alaskan earthquake, *Pure Appl. Geophys.*, *154*, 593-632.

Ehlers, T.A. and K.A. Farley (2003), Apatite (U-Th)/He thermochronometry: Methods and applications to problems in tectonic and surface processes, *Earth Planet. Sci. Lett.*, *206*, 1-14.

Ehlers, T.A., K.A. Farley, M.E. Rusmore, and G.J. Woodsworth (2006), Apatite (U-Th)/He signal of large-magnitude accelerated glacial erosion, southwest British Columbia, *Geology*, *34*, 765-768.

El-Fiky, G. and T. Kato (2006), Secular crustal deformation and interplate coupling of the Japanese Islands as deduced from continuous GPS array, 1996-2001, *Tectonophysics*, *422*, 1-22.

Farley, K.A. (2000), Helium diffusion from apatite: General behavior as illustrated by Durango fluorapatite, *J. Geophys. Res.*, *105*, 2903-2914.

Farley, K.A., M.E. Rusmore, and S.W. Bogue (2001), Post-10 Ma uplift and exhumation of the northern Coast Mountains, British Columbia, *Geology*, *29*, 99-102.

Fisher, D.M., T.W. Gardner, J.S. Marshall, P.B. Sak, and M. Protti (1998), Effect of subducting sea-floor roughness on fore-arc kinematics, Pacific coast, Costa Rica, *Geology*, *26*, 467-470.

Flores, C., and D.I. Doser (2005), Shallow seismicity of the Anchorage, Alaska, region (1964-1999), *Bull. Seismol. Soc. Am.*, *95*, 1865-1879.

Freitag, R., C. Gaedicke, B. Baranov, and N. Tsukanov (2001), Collisional processes at the junction of the Aleutian-Kamchatka arcs: new evidence from fission track analysis and field observations, *Terra Nova*, *13*, 433-442.

Freymueller, J.T., S.C. Cohen, and H.J. Fletcher (2000), Spatial variations in present-day deformation, Kenai Peninsula, Alaska, and their implications, *J. Geophys. Res.*, *105*, 8079-8101.

Fruehn, J., R. von Huene, and M.A. Fisher (1999), Accretion in the wake of terrane collision: The Neogene accretionary wedge off Kenai Peninsula, Alaska, *Tectonics*, *18*, 263-277.

Fuis, G.S. and G. Plafker (1991), Evolution of deep structure along the Trans-Alaska Crustal Transect, Chugach Mountains and Copper River basin, southern Alaska, *J. Geophys. Res.*, *96*, 4229-4253.

Fuller, C.W., S.D. Willett, and M.T. Brandon (2006), Formation of forearc basins and their influence on subduction zone earthquakes, *Geology*, *34*, 65-68.

Gräfe, K., W. Frisch, I.M. Villa, and M. Meschede (2002), Geodynamic evolution of southern Costa Rica related to low-angle subduction of the Cocos Ridge: constraints from thermochronology, *Tectonophysics*, *348*, 187-204.

Gutscher, M.-A. (2002), Andean subduction styles and their effect on thermal structure and interplate coupling, *J. South Am. Earth Sci.*, *15*, 3-10.

Gutscher, M.-A., W. Spakman, H. Bijwaard, and E.R. Engdahl (2000), Geodynamics of flat subduction: Seismicity and tomographic constraints from the Andean margin, *Tectonics*, *19*, 814-833.

Haeussler, P.J., R.L. Bruhn, and T.L. Pratt (2000), Potential seismic hazards and tectonics of upper Cook Inlet basin, Alaska, based on analysis of Pliocene and younger deformation, *Geol. Soc. Am. Bull.*, *112*, 1414-1429.

Hager, B.H. (1984), Subducted slabs and the geoid: Constraints on mantle rheology and flow, *J. Geophys. Res.*, *89*, 6003-6015.

Hasebe, N. and T. Tagami (2001), Exhumation of an accretionary prism--results from fission track thermochronoloy of the Shimanto Belt, southwest Japan, *Tectonophysics*, *331*, 247-267.

Hasegawa, A., A. Yamamoto, N. Umino, S. Miura, S. Horiuchi, D. Zhao, and H. Sato (2000), Seismic activity and deformation process of the overriding plate in the northeastern Japan subduction zone, *Tectonophysics*, *319*, 225-239.

Haeuselmann, P., D.E. Granger, P.-Y. Jeannin, and S.-E. Lauritzen (2007), Abrupt glacial valley incision at 0.8 Ma dated from cave deposits in Switzerland, *Geology*, *35*, 143-146.

Hebbeln, D., F. Lamy, M. Mohtadi, and H. Echtler (2007), Tracing the impact of glacial-interglacial climate variability on erosion of the southern Andes, *Geology*, *35*, 131-134.

Husson, L. (2006), Dynamic topography above retreating subduction zones, *Geology*, *34*, 741-744.

Johnsson, M.J., M.J. Pawlewicz, A.G. Harris, and Z.C. Valin (1992), Vitrinite reflectance and conodont color alteration index data from Alaska: Data to accompany the thermal maturity map of Alaska, *U.S. Geol. Surv.*, Report OF 92-0409.

Johnsson, M.J. and D.G. Howell (1996), Thermal maturity of sedimentary basins in Alaska: An overview, *U.S. Geol. Surv. Bull.*, Report B 2142, 1-9.

Kelsey, H.M., D.C. Engebretson, C.E. Mitchell, and R.L. Ticknor (1994), Topographic form of the Coast Ranges of the Cascadia Margin in relation to coastal uplift rates and plate subduction, *J. Geophys. Res.*, *99*, 12,245-12,255.

Lahr, J.C. and G. Plafker (1980), Holocene Pacific-North American plate interaction in southern Alaska: Implications for the Yakataga seismic gap, *Geology*, *8*, 483-486.

Larsen, C.F., R.J. Motyka, J.T. Freymueller, K.A. Echelmeyer, and E.R. Ivins (2005), Rapid viscoelastic uplift in southeast Alaska caused by post-Little Ice Age glacial retreat, *Earth Planet. Sci. Lett.*, *237*, 548-560.

Little, T.A. and C.W. Naeser (1989), Tertiary tectonics of the Border Ranges fault system, Chugach Mountains, Alaska: Deformation and uplift in a forearc setting, *J. Geophys. Res.*, *94*, 4333-4359.

Magoon, L.B. (1986), Present-day geothermal gradient, *U.S. Geol. Surv. Bull.*, Report B 1596, 41-46.

Malloy, R.J. (1964), Crustal uplift southwest of Montague Island, Alaska, *Science*, *146*, 1048-1049.

Mazzotti, S., H. Dragert, R.D. Hyndman, M.M. Miller, J.A. Henton (2002), GPS deformation in a region of high crustal seismicity: N. Cascadia forearc, *Earth Planet. Sci. Lett.*, *198*, 41-48.

McDowell, F.W., W.C. McIntosh, and K.A. Farley (2005), A precise $^{40}Ar/^{39}Ar$ reference age for the Durango apatite (U-Th)/He and fission-track dating standard, *Chem. Geol.*, *214*, 249-263.

McQuarrie, N., B.K. Horton, G. Zandt, S. Beck, and P.G. DeCelles (2005), Lithospheric evolution of the Andean fold-thrust belt, Bolivia, and the origin of the central Andean Plateau, *Tectonophysics*, *399*, 15-37.

Miller, M.M., D.J. Johnson, C.M. Rubin, H. Dragert, K. Wang, A. Qamar, and C. Goldfinger (2001), GPS-determination of along-strike variation in Cascadia margin kinematics: Implications for relative plate motion, subduction zone coupling, and permanent deformation, *Tectonics*, *20*, 161-176.

Pavlis, T.L., C. Picornell, L. Serpa, R.L. Bruhn, and G. Plafker (2004), Tectonic processes during oblique collision: Insights from the Saint Elias Orogen, northern North American Cordillera, *Tectonics*, *23*, 14 p.

Péwé, T.L. (1975), Quaternary geology of Alaska, *U.S. Geol. Surv. Prof. Paper*, Report P 835, 145 p.

Plafker, G., J.C. Moore, and G.R. Winkler (1994), Geology of the southern Alaska margin, in *The Geology of Alaska*, edited by G. Plafker and H.C. Berg, *Geol. Soc. Am.*, *Geology of North America*, *G-1*, 389-449.

Plafker, G., W.J. Nokleberg, and J.S. Lull (1989), Bedrock geology and tectonic evolution of the Wrangellia, Peninsular, and Chugach terranes along the Trans-Alaska Crustal Transect in the Chugach Mountains and southern Copper River basin, Alaska, *J. Geophys. Res.*, *94*, 4255-4295.

Prawirodirdjo, L., Y. Bock, R. McCaffrey, J. Genrich, E. Calais, C. Stevens, S.S.O. Puntodewo, C. Subarya, J. Rais, P. Zwick, and Fauzi (1997), Geodetic observations of interseismic strain segmentation at the Sumatra subduction zone, *Geophys. Res. Lett.*, *24*, 2601-2604.

Ratchkovski, N.A. and R.A. Hansen (2002), New evidence for segmentation of the Alaska subduction zone, *Bull. Seis. Soc. Am.*, *92*, 1754-1765.

Reiners, P.W. and M.T. Brandon (2006), Using thermochronology to understand orogenic erosion, *Ann. Rev. Earth Planet. Sci.*, *34*, 419-466.

Reiners, P.W., T.A. Ehlers, S.G. Mitchell, and D.R. Montgomery (2003), Coupled spatial variations in precipitation and long-term erosion rates across the Washington Cascades, *Nature*, *426*, 645-647.

Shuster, D.L., T.A. Ehlers, M.E. Rusmore, and K.A. Farley (2005), Rapid glacial erosion at 1.8 Ma revealed by $^{4}He/^{3}He$ thermochronometry, *Science*, *310*, 1668-1670.

Song, T.-R.A. and M. Simons (2003), Large trench-parallel gravity variations predict seismogenic behavior in subduction zones, *Science*, *301*, 630-633.

Spotila, J.A., J.T. Buscher, A.J. Meigs, and P.W. Reiners (2004), Long-term glacial erosion of active mountain belts: Example of the Chugach-St. Elias Range, Alaska, *Geology*, *32*, 501-504.

Trenkamp, R., J.N. Kellogg, J.T. Freymueller, and H.P. Mora (2002), Wide plate margin deformation, southern Central America and northwestern South America, CASA GPS observations, *J. South Am. Earth Sci.*, *15*, 157-171.

Veilleux, A.M. and D.I. Doser (2007), Studies of Wadati-Benioff zone seismicity of the Anchorage, Alaska, region, *Bull. Seis. Soc. Am.*, *97*, 52-62.

Westbrook, G.K., J.W. Ladd, P. Buhl, N. Bangs, and G.J. Tiley (1988), Cross section of an accretionary wedge: Barbados Ridge complex: *Geology*, *16*, 631-635.

White, J.M., T.A. Ager, D.P. Adam, E.B. Leopold, G. Liu, H. Jetté, and C.E. Schweger (1997), An 18 million year record of vegetation and climate change in northwestern Canada and Alaska: tectonic and global climatic correlates, *Palaeogeography, Palaeoclimatology, Palaeoecology*, *130*, 293-306.

Wolf, R.A., K.A. Farley, and L.T. Silver (1996), Helium diffusion and low-temperature thermochronometry of apatite, *Geochim. Cosmochim. Acta*, *60*, 4231-4240.

Zweck, C., J.T. Freymueller, and S.C. Cohen (2002), Three-dimensional elastic dislocation modeling of the postseismic response to the 1964 Alaska earthquake, *J. Geophys. Res.*, *107*, B42064, 12 p.

Table 3.1: AHe data.

Sample	Elev. (m)	Latitude	Longitude	Lithology	# Grains	Mass (mg)	Ft	U ppm	Th ppm	MWAR	He pmol	Age (Ma)	Avg. (Ma)	% SD
99CH1-4*	46	60.4779°	-145.3375 °	granodiorite	18	0.01292	0.630	36.2	10.0	33.5	0.0237	*14.5*	**7.0±1.0**	±13.8%
-6*					19	0.0153	0.621	30.5	9.11	35.7	0.0137	**8.4**		
-1A*					19	0.0173	0.632	30.7	8.53	35.1	0.0121	**6.5**		
-1B*					19	0.0252	0.676	28.2	9.28	38.1	0.0168	**6.2**		
01CH3-2	701	61.1694°	-145.7188°	schist	5	0.00593	0.682	36.3	41.4	39.4	0.0162	**16.6**	**12.7±1.3**	±10.4%
-3					5	0.00670	0.723	14.4	26.6	42.0	0.0108	**20.6**		
-4					5	0.00713	0.691	14.8	25.8	41.8	0.0098	**18.2**		
-5					5	0.00900	0.750	47.0	39.6	49.2	0.0321	**16.1**		
01CH4-3	1417	61.5346°	-145.3263°	metagraywacke	1	0.00285	0.730	3.5	9.3	50.6	0.0035	*54.8*	**38.5±2.1**	±5.5%
-4					6	0.00470	0.643	6.6	18.6	34.9	0.0064	**36.4**		
-5					6	0.00426	0.645	5.1	13.7	33.1	0.0044	**36.7**		
-6					6	0.00412	0.614	13.0	16.2	33.7	0.0088	**39.5**		
-7					3	0.00436	0.678	6.3	19.0	40.9	0.0070	**41.6**		
01CH8-1*	1174	61.2979°	-145.3206°	metagraywacke	17	0.00674	0.558	19.6	29.6	28.5	0.0136	**25.8**	**23.7±1.5**	±6.3%
-2					4	0.00304	0.666	53.9	55.7	33.4	0.0154	**21.7**		
-3					5	0.00441	0.688	44.1	45.9	38.3	0.0213	**24.4**		
-4					5	0.00506	0.682	18.0	32.6	37.8	0.0113	**24.1**		
-5					5	0.00510	0.690	37.0	41.2	41.2	0.0193	**22.3**		
01CH10-4	671	61.0712°	-145.9888°	schist	6	0.00374	0.598	45.9	59.0	31.9	0.0080	**11.4**	**11.5±0.3**	±2.3%
-5					6	0.00507	0.666	16.4	27.1	37.7	0.0067	*16.4*		
-6					6	0.00427	0.646	37.7	32.9	34.9	0.0074	**11.2**		
-7					5	0.00431	0.644	15.8	18.7	36.3	0.0035	**11.9**		
01CH28-1*	564	60.4926°	-145.2510°	granite	24	0.02127	0.630	27.1	6.60	34.6	0.0114	**5.7**	**5.76±0.3**	±5.4%
-2*					17	0.02844	0.715	24.7	7.72	45.8	0.0146	**5.2**		
-3					5	0.00937	0.721	34.2	9.3	45.2	0.0078	**6.06**		
-4					5	0.00670	0.668	36.4	8.7	39.4	0.0054	**6.02**		
-5					5	0.00808	0.683	36.2	9.7	42.5	0.0065	**5.83**		
02CH17-1	1417	61.0708°	-145.1978°	graywacke	11	0.0166	0.713	29.9	18.0	44.9	0.0393	**18.6**	**18.1±1.8**	±10.2%
-2					5	0.0175	0.784	7.6	9.3	71.9	0.0114	**16.2**		
-3					7	0.0170	0.737	5.9	10.7	55.0	0.0133	*24.0*		
-4					8	0.0113	0.705	23.5	15.3	45.1	0.0188	**16.6**		
-5					8	0.0121	0.687	24.1	30.6	43.8	0.0285	**20.8**		
02CH38-1*	457	60.6935°	-146.0412°	granite	22	0.0163	0.642	20.1	32.8	37.3	0.0075	**4.9**	**4.77±0.8**	±16.6%
-2*					16	0.00978	0.612	19.4	31.3	32.7	0.0179	*21.2*		
-3					4	0.00470	0.704	14.2	18.1	37.1	0.0019	**6.04**		
-4					5	0.00403	0.645	18.5	27.6	35.1	0.0013	**3.69**		
-5					4	0.00338	0.640	14.0	21.0	32.2	0.0009	**4.23**		
-6					5	0.00410	0.678	26.1	27.2	34.2	0.0024	**4.97**		
02CH39-1*	244	61.7754°	-148.5029°	granite	16	0.0230	0.729	5.13	6.12	44.5	0.0135	**23.3**	**25.2±1.8**	±7.4%
-2*					15	0.0178	0.702	5.05	5.98	40.7	0.0114	**27.0**		

Table 3.1: cont.

Sample	Elev. (m)	Latitude	Longitude	Lithology	# Grains	Mass (mg)	Ft	U ppm	Th ppm	MWAR	He pmol	Age (Ma)	Avg. (Ma)	% SD
06STP75-1	223	61.7762°	-148.5007°	granite	5	0.0158	0.758	8.0	10.0	48.7	0.0128	**19.7**	**18.1±3.9**	±21.8%
-2					8	0.0176	0.743	8.2	9.5	45.4	0.0116	**16.3**		
-3					7	0.0153	0.737	6.7	8.7	46.9	0.0067	**12.9**		
-4					3	0.0218	0.826	7.3	8.7	69.8	0.0207	**23.5**		
06STP76-1	23	60.1041°	-149.3612°	turbidite	4	0.0069	0.744	43.2	80.0	47.2	0.0219	**13.1**	**13.5±0.8**	±6.2%
-2					5	0.0066	0.713	11.2	26.9	43.5	0.0061	**13.9**		
-3					7	0.0117	0.739	30.1	34.6	49.2	0.0229	**13.2**		
-4					6	0.0128	0.758	60.7	92.8	54.3	0.0523	**12.4**		
-5					6	0.0067	0.693	9.2	25.7	40.8	0.0056	**14.9**		
06STP77-1	15	60.7759°	-148.7096°	granite	10	0.0068	0.625	10.8	4.0	34.2	0.0100	*38.3*	**14.9±1.2**	±8.2%
-2					12	0.0076	0.623	4.6	3.4	33.2	0.0023	**16.9**		
-3					8	0.0163	0.738	0.8	2.6	51.7	0.0013	**14.3**		
-4					5	0.0112	0.764	21.1	15.2	54.0	0.0152	**13.7**		
-5					2	0.0132	0.844	26.2	11.1	76.0	0.0245	**14.6**		
06STP78-1	15	61.0318°	-149.7620°	turbidite	8	0.0101	0.708	4.3	11.0	42.4	0.0058	**22.6**	**22.0±1.7**	±7.8%
-2					6	0.0155	0.779	2.3	6.8	57.0	0.0048	**19.4**		
-3					6	0.0114	0.736	3.5	9.1	48.4	0.0058	**22.9**		
-4					5	0.0180	0.814	4.8	8.4	64.6	0.0109	**20.9**		
-5					3	0.0109	0.777	3.0	8.3	59.0	0.0054	**24.3**		
06STP79-1	102	60.4863°	-150.0463°	turbidite	4	0.0037	0.657	61.4	48.7	38.5	0.0100	**10.8**	**19.9±7.6**	±38.4%
-2					8	0.0034	0.551	18.0	27.4	27.9	0.0028	**11.7**		
-3					4	0.0050	0.690	19.4	33.1	40.6	0.0150	**30.4**		
-4					3	0.0048	0.707	10.2	17.2	44.3	0.0055	**21.4**		
-5					2	0.0057	0.730	6.6	4.5	51.1	0.0042	**25.3**		

*Run in 2002-2003. All other age measurements are from 2007.
Ages in italics were considered outliers and not used for average age calculation

Figures

Figure 3.1: Major tectonic features of the Kenai, Chugach, St. Elias, and Fairweather Mountains, plotted on a shaded relief map from a 60 m digital elevation model (USGS). Major active faults are shown as solid lines. Major inactive thrust faults and terrane boundaries are shown as solid lines with open teeth. Fault and geologic data from *Plafker et al.* [1994], *Bruhn et al.* [2004], *Bruhn and Haeussler* [2006], *Berger et al.* [in prep.], and *McAleer and Spotila* [in prep.]. Lines indicate the locations of cross section and profiles in Figures 3.3 and 3.5. Plate motion vector from *Lahr and Plafker* [1980], *DeMets et al.* [1990], and *Plafker et al.* [1994].

Figure 3.1: Tectonic structures of Kenai, Chugach, St. Elias, and Fairweather Mountains, southern Alaska.

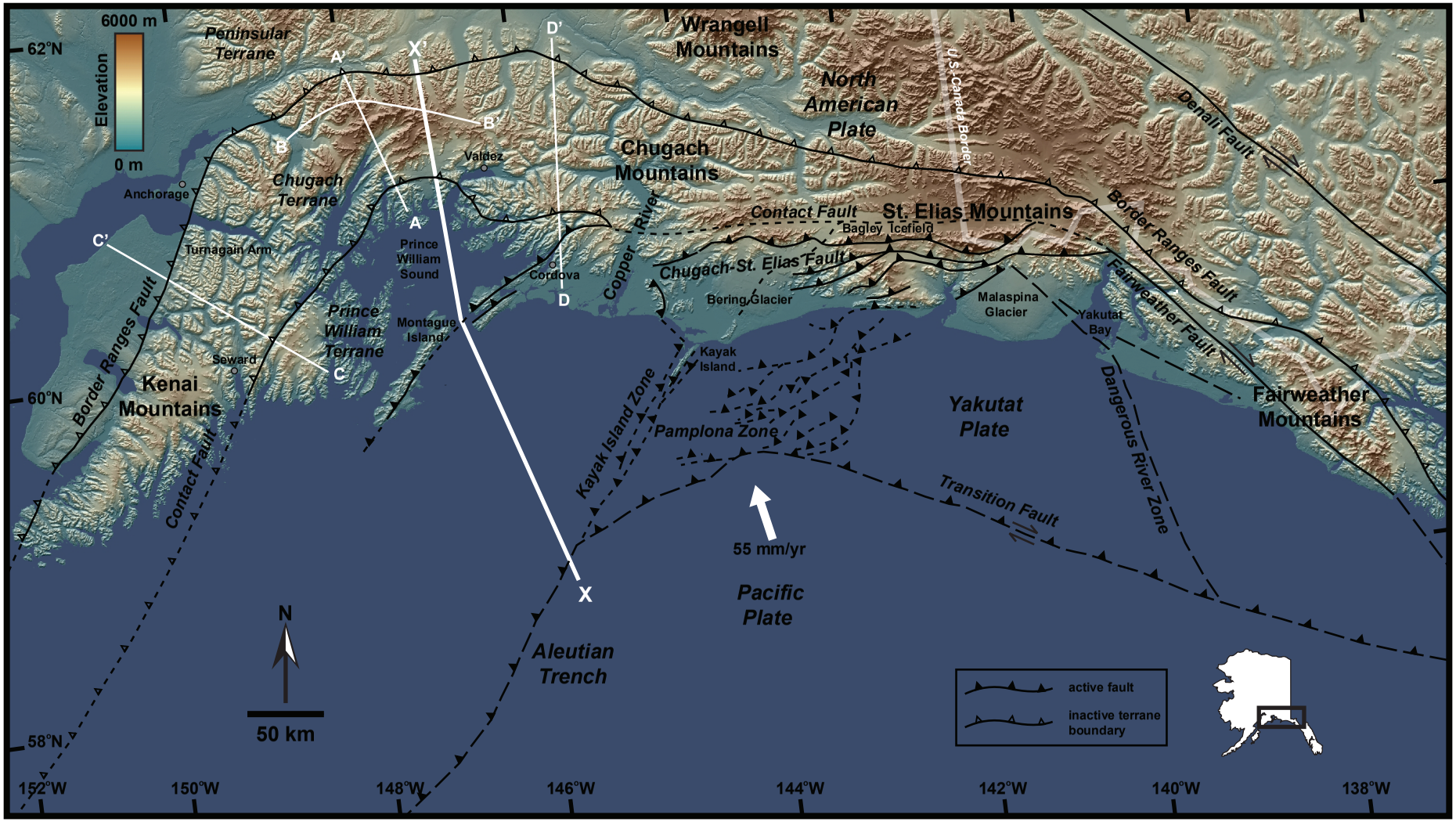

Figure 3.2: Three-dimensional image of topography looking southeast at Chugach and Kenai Mountains across Cook Inlet. Image created from 60 m digital elevation model (USGS) using ArcScene. Red points represent sample locations from this study with corresponding AHe ages. Fault data and plate motion vector from Figure 3.1.

Figure 3.2: Topography of Chugach and Kenai Mountains as viewed across Cook Inlet.

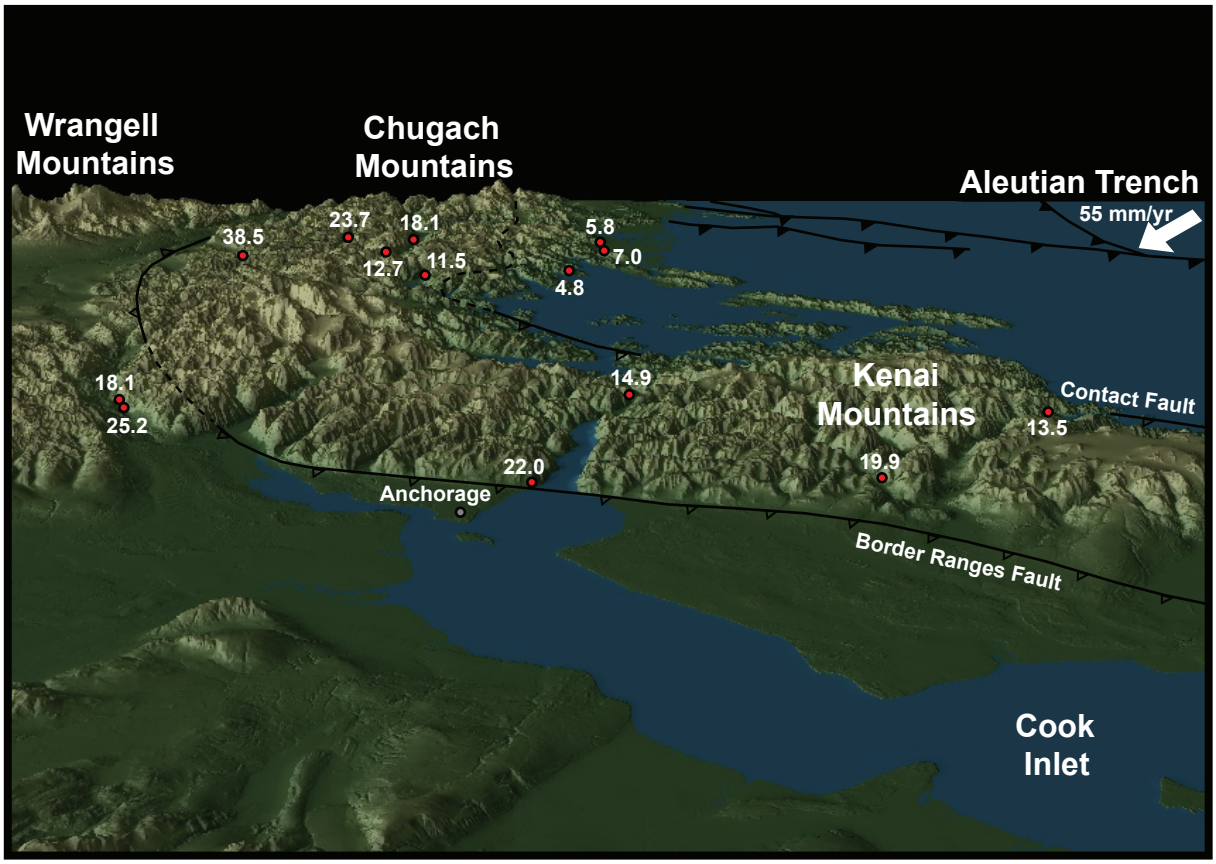

Figure 3.3: Cross section of the Aleutian megathrust, showing approximate boundaries of the Prince William, Chugach, and Peninsular terranes. Location of section is shown in Figure 3.1. Synthesis of data from *Plafker et al.* [1994].

Figure 3.3: Cross section showing Aleutian subduction zone and accreted terranes.

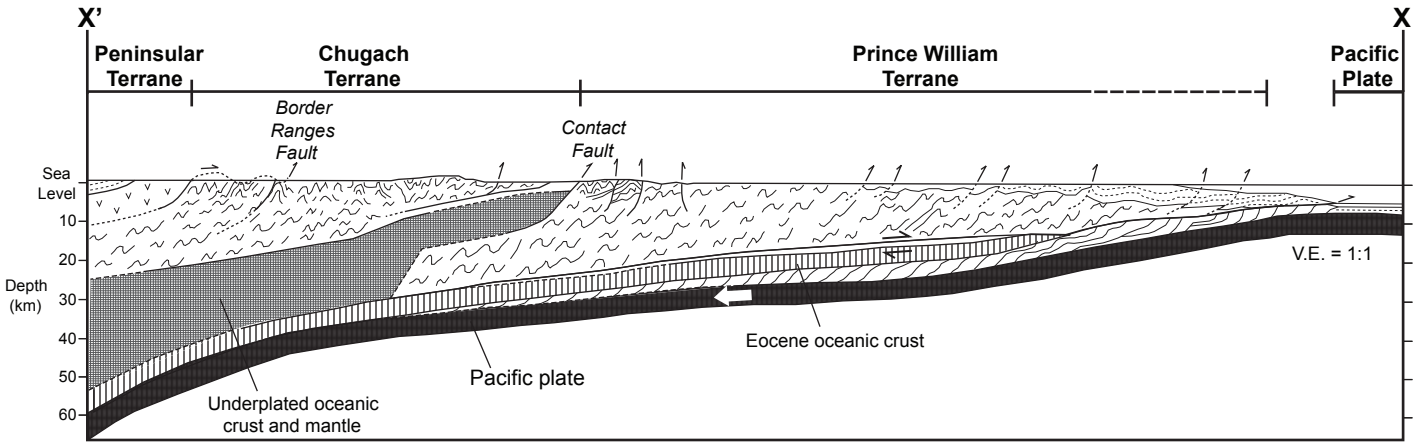

Figure 3.4: Slope map for Kenai, Chugach, and St. Elias Mountains. Slope determined by analyzing 60 m digital elevation models (USGS) using ArcGIS, where slope is calculated from elevation difference between one cell and eight surrounding cells. White dashed lines show outline of areas analyzed for peak and average elevation and slope as discussed in the text. The area between Copper River and Yakutat Bay (location shown in Figure 3.1) was analyzed without the Bering and Malaspina piedmont glaciers.

Figure 3.4: Slope map of the Chugach and Kenai Mountains.

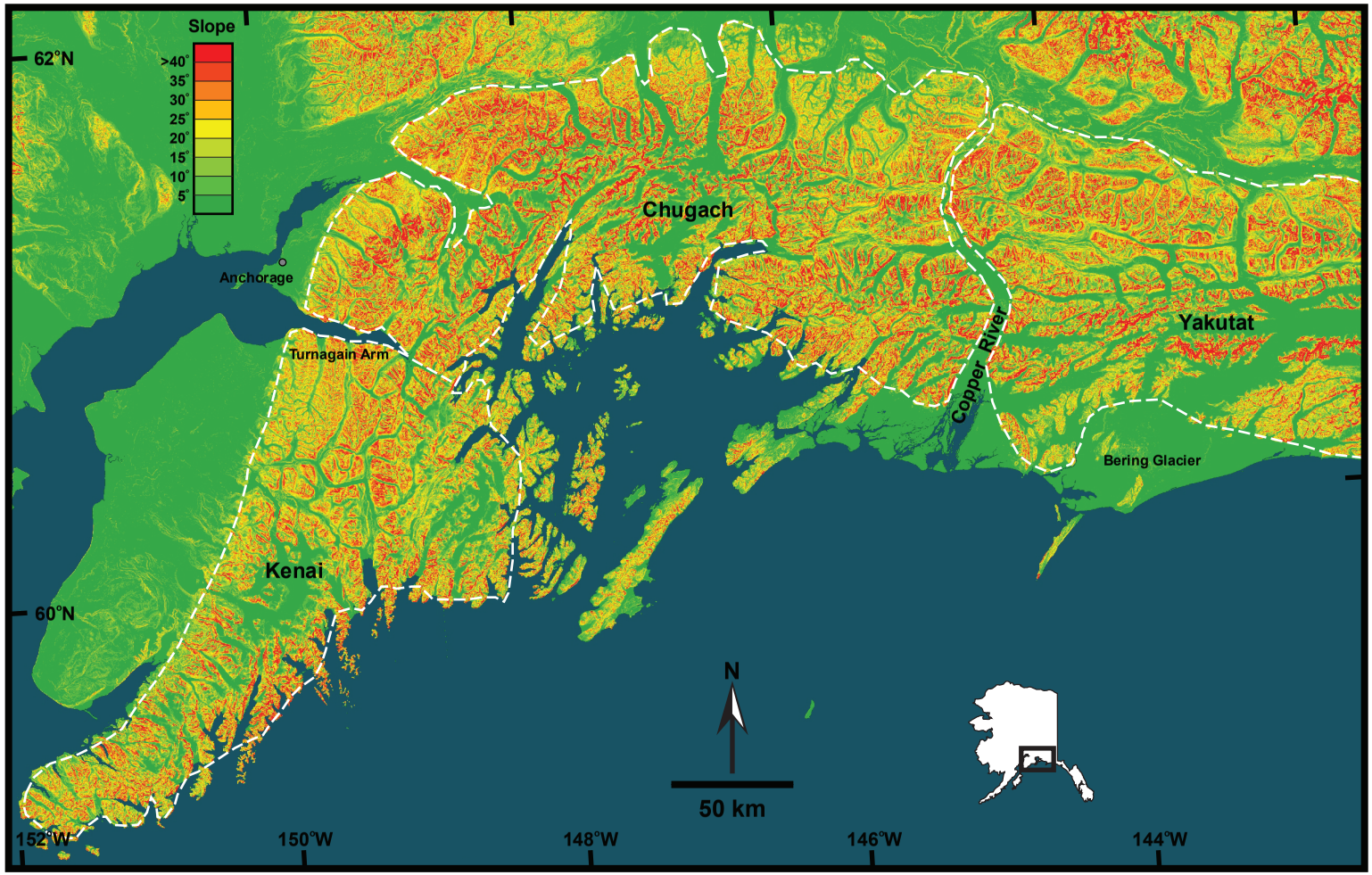

Figure 3.5: Along-strike (BB') and across-strike (AA', CC', and DD') elevation profiles in the Chugach-Kenai Mountains. Locations of profiles are shown in Figure 3.1. AHe sample locations and ages are shown, including three from *Spotila et al.* [2004]. A) Topographic profile along AA', running northwest-southeast across the axis of the Chugach Mountains just north of Prince William Sound. Note the large, massif-like mass of high elevation and the south-facing escarpment. B) Topographic profile along BB', running east and west along strike from the area of profile AA'. Topography decreases irregularly in either direction. C) Topographic profile across the Kenai Mountains. The dashed line is an imaginary surface drawn as an envelope to connect the maximum peak elevations, which illustrates the rough concordance of peak heights. This surface tilts down to the northwest. D) Topographic profile across the eastern Chugach Mountains. The dashed line represents an envelope of the maximum peak heights, as described above.

Figure 3.5: Across-strike and along-strike elevation profiles from the Chugach and Kenai Mountains.

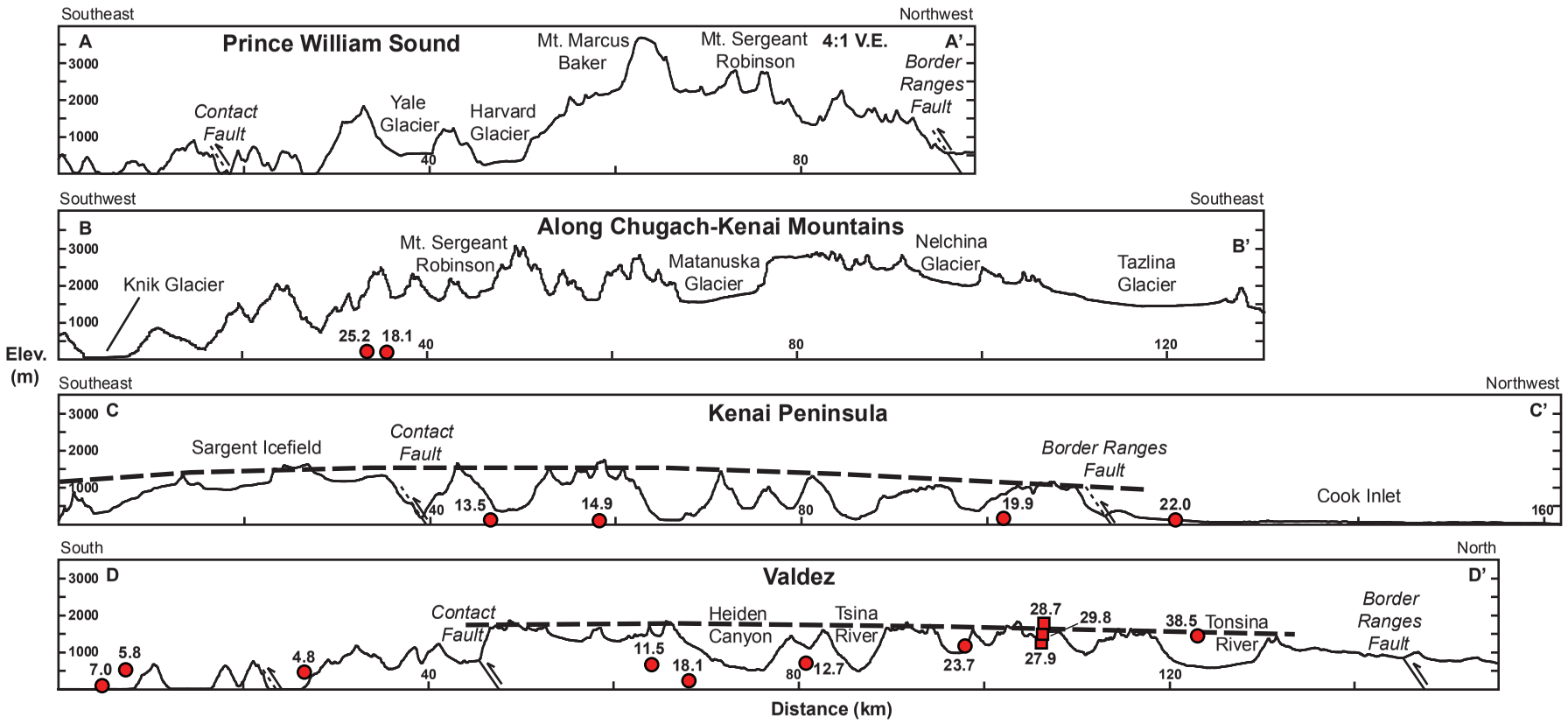

Figure 3.6: Distribution of AHe ages plotted on a shaded relief map from a 60 m digital elevation model (USGS). Data includes three AHe ages from *Spotila et al.* [2004], shown as squares. The two areas illustrated by yellow circles represent the locations where previous AFT ages have been measured by *Little and Naeser* [1989] and *Plafker et al.* [1989], which are generally in the range of 17-42 Ma.

Figure 3.6: Distribution of AHe and AFT ages.

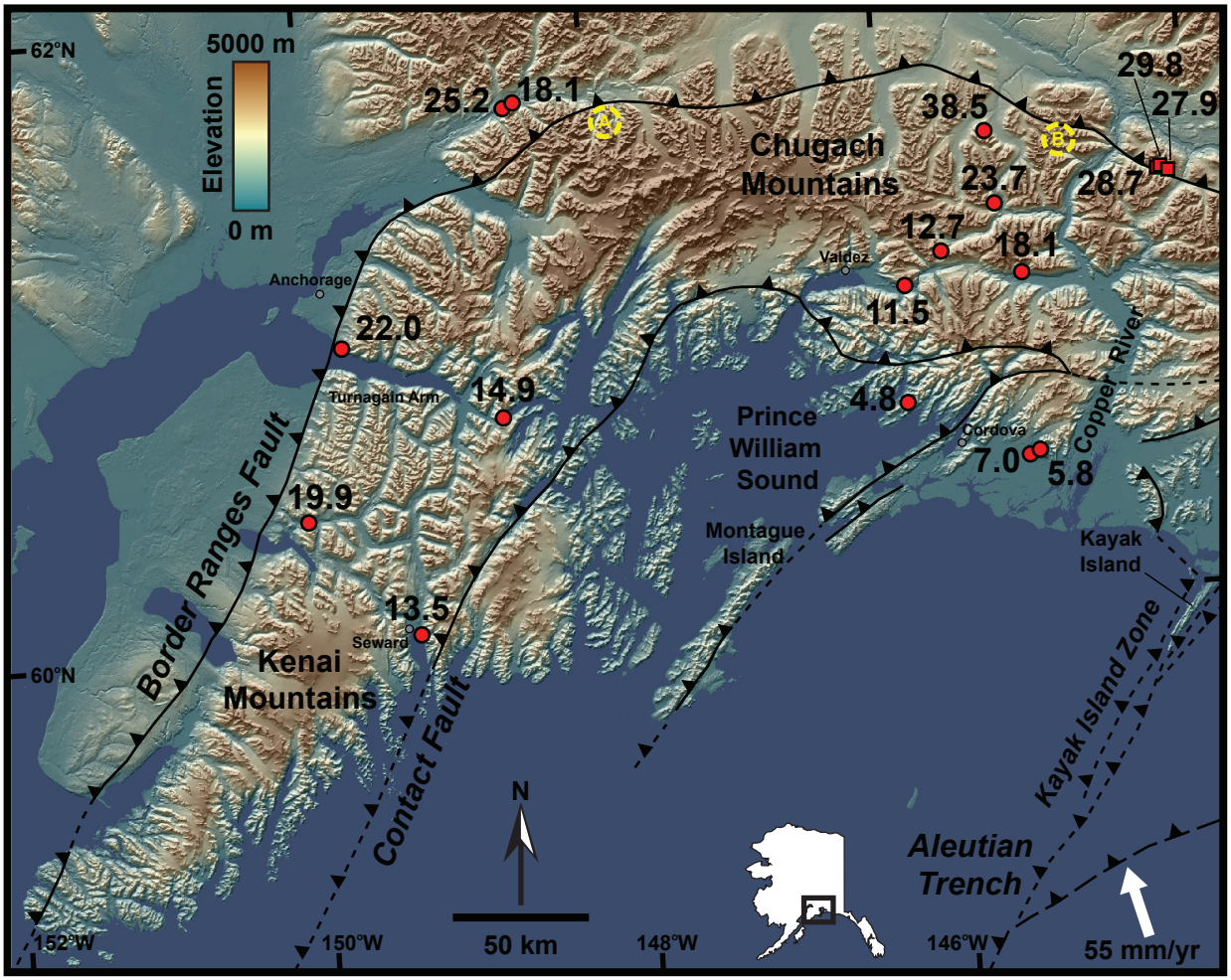

Figure 3.7: A) Plot of AHe age vs. distance, showing a distinct increase in age with distance from the coast in both the Kenai area and the Chugach Mountains near Valdez. B) Plot of elevation vs. AHe age, showing a distinct increase in age with increasing elevation in the Valdez area, but not in the Kenai Mountains. Closed circles = Valdez area (east of Valdez); open circles = Kenai area (west of Valdez); diamonds = ages from near the Copper River from *Spotila et al.* [2004]. Regression line includes all samples near Valdez, including those from *Spotila et al.* [2004]. Error bars represent estimated 10% error for AHe ages.

Figure 3.7: (a) AHe age vs. Distance from Coast; (b) Elevation vs. AHe age.

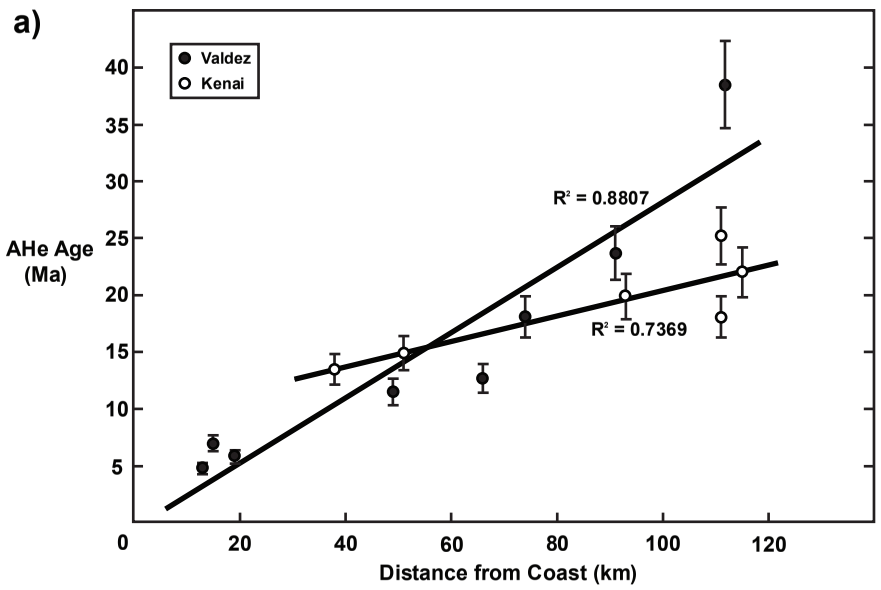

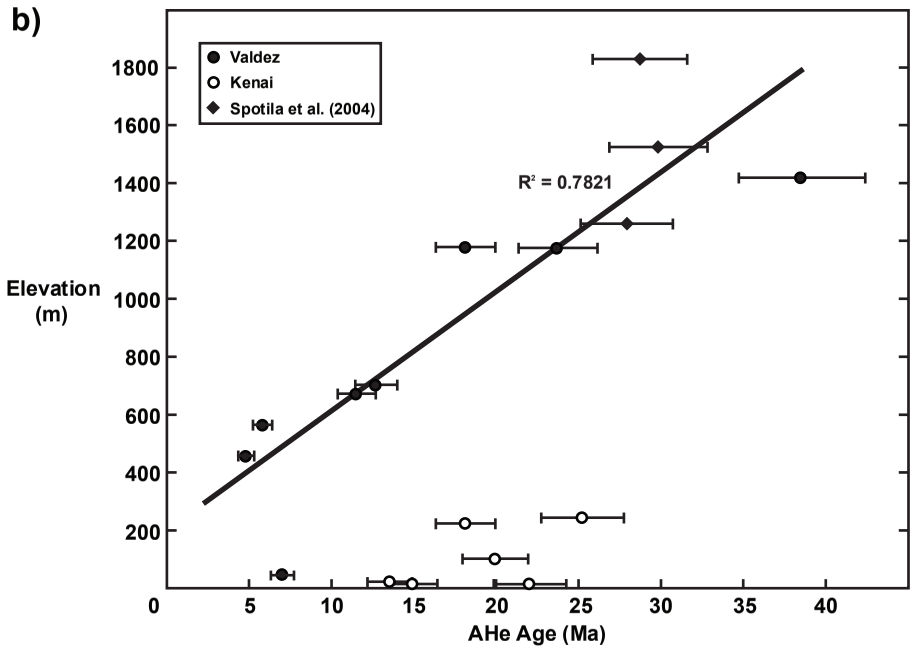

Vita

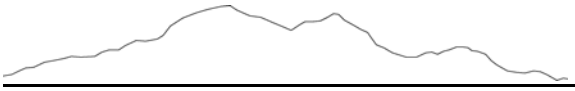

Jamie Todd Buscher

EDUCATION

Doctorate of Philosophy, Geology, May 2007
Virginia Tech, Blacksburg, VA
Dissertation: Long-term exhumation of landscapes along the Pacific-North American plate boundary as inferred from apatite (U-Th)/He and ArcGIS analyses.
Advisor: Dr. James A. Spotila

Master of Science, Geology, October 2003
Virginia Tech, Blacksburg, VA
Thesis: The impact of long-term glacial erosion on the active Chugach-St. Elias Mountains, southern Alaska. Advisor: Dr. James A. Spotila

Bachelor of Science, Geology, September 1998
University of California, Los Angeles (UCLA), Los Angeles, CA

Pasadena City College, Pasadena, CA, Spring 1992 to Summer 1995

RESEARCH EXPERIENCE

Doctoral Research, Virginia Tech, Spring 2004 to Spring 2007
Studied the influence of transpression and convergence along the Pacific-North American plate boundary on uplift of the northern San Gabriel and Chugach-Kenai Mountains by constraining the exhumation pattern inferred from apatite (U-Th)/He data and ArcGIS topographic analyses.

Masters Research, Virginia Tech, Fall 2001 to Fall 2003
Studied the influence of glacial erosion on mountain building in the Chugach-St. Elias Mountains, southern Alaska, by constraining the exhumation pattern with apatite (U-Th)/He data.

Research Assistant, Virginia Tech, Spring 2002; Fall 2004

RELATED EXPERIENCE

Field Assistant, ground-penetrating radar study along the North Frontal thrust system, San Bernardino Mountains, southern California, while at Virginia Tech. Acknowledged in Anderson et al. (2003).

Field Assistant, structural geology study of the Altyn Tagh fault, northwest China, while at UCLA. Acknowledged in Cowgill et al. (2000).

TEACHING EXPERIENCE

Teaching Assistant, Elements of Structural Geology, Spring 2007
Virginia Tech

Teaching Assistant Coordinator, Physical Geology Laboratory, Fall 2006
Virginia Tech

Teaching Assistant, Physical Geology Laboratory, Fall 2001, 2002, 2006; Spring 2006
Virginia Tech

Teaching Assistant, Geoscience Field Observations, Spring 2003, 2004, 2005
Virginia Tech

EMPLOYMENT HISTORY

Staff Geologist, November, 1998 to July, 2001
Hydrologue, Inc., Pasadena, CA
Consulting Engineers and Geologists

Field Duties:

- Geotechnical sampling for soil stability and liquefaction studies
- Trenching and continuous core sampling for fault studies
- Field density tests and foundation inspections for proposed residential and commercial developments
- Geologic mapping for hillside developments
- Groundwater sampling and monitoring for analysis of toxins released by fuel tanks and industrial machinery
- Fuel tank excavation and soil sampling

Office Duties:

- Soil engineering laboratory tests: shear strength, consolidation, expansion, maximum density, Atterberg limits, sieve analysis, and specific gravity
- Report preparation for soil engineering, geology, compaction, and percolation studies

PUBLICATIONS

Buscher, J.T., A.L. Berger, and J.A. Spotila (*submitted*), Exhumation in the Chugach-Kenai Mountain belt above the Aleutian subduction zone, southern Alaska, *AGU Chapman Monograph*.

Spotila, J.A., N.A. Niemi, R.C. Brady, M.A. House, **J.T. Buscher,** and M. Oskin (*submitted*), Long-term continental deformation associated with transpressive plate motion: The San Andreas fault, *Geology*.

Buscher, J.T. and J.A. Spotila *(submitted),* Near-field response to transpression along the southern San Andreas fault, based on exhumation of the northern San Gabriel Mountains, southern California, *Tectonics*.

Spotila, J.A., M.A. House, N.A. Niemi, R.C. Brady, M. Oskin, and **J.T. Buscher** (*in press*), Mechanisms of transpression along the San Andreas fault, based on patterns of bedrock uplift, *GSA Special Paper*.

Spotila, J.A., **J.T. Buscher,** A.J. Meigs, and P.W. Reiners (2004), Long-term glacial erosion of active mountain belts: Example of the Chugach/St. Elias Range, Alaska, *Geology*, *32*, 501-504.

ABSTRACTS AND PRESENTATIONS

Buscher, J.T. and J.A. Spotila (2006), The character of transpressive deformation along the southern San Andreas fault, based on exhumation of the northern San Gabriel Mountains, southern California, *Eos Transactions AGU 87*, Suppl. T43D-1671.

Buscher, J.T. and J.A. Spotila (2006), Heterogeneous exhumation along the southern San Andreas fault as inferred from (U-Th)/He ages in the northern San Gabriel Mountains, southern California, *GSA Abstracts with Programs, 38, 449.*

Buscher, J.T. and J.A. Spotila (2005), Transpressive block exhumation along the San Andreas fault in the northwestern San Gabriel Mountains, *GSA Abstracts with Programs, 37*, 346.

Buscher, J.T., J.A. Spotila, and A. Meigs (2002), Glacial erosion as a primary control on landscape evolution of the active Chugach/St. Elias Range of southern Alaska, *Eos Transactions AGU 83*, Suppl. T71B-1173.

Spotila, J.A. and **J.T. Buscher** (2002), Measuring crustal convergence using rock exhumation along the complex glaciated Chugach Mountains, southeast Alaska, *Eos Transactions AGU 83*, Suppl. F1361.

Spotila, J.A., **J.T. Buscher,** and A. Meigs (2002), The influence of glacial erosion on active mountain building, based on exhumation of the Chugach/St. Elias Range, southeast Alaska, *GSA Abstracts with Programs, 34*, 78.

PROFESSIONAL AFFILIATIONS

American Geophysical Union
Geological Society of America

GRANTS AND AWARDS

Chevron-Texaco Graduate Fellowship Award, Summer 2007, Department of Geosciences, Virginia Tech, summer research assistantship awarded from the Chevron-Texaco Scholarship Fund.

Geosciences Outstanding Service Recognition Award, May 2007, Department of Geosciences, Virginia Tech, to honor exceptional leadership and selfless contributions of students to the department

Geological Society of America Graduate Student Research Grant, Spring 2006, for proposal entitled "Inferring earthquake recurrence for the Nicoya segment of the Cocos plate, Costa Rica."

Travel Fund Program Grant, Graduate Student Assembly, Virginia Tech, to cover travel expenses for Geological Society of America Annual Meeting, Salt Lake City, Fall 2005.

CERTIFICATE

Future Professoriate Graduate Certificate, Virginia Tech
Certificate program offered by Graduate School, designed to prepare graduate students for faculty positions.